Mixed-state topological order parameters for symmetry-protected fermion matter

Ze-Min Huang [1,2] and Sebastian Diehl[1]
[1]Institute for Theoretical Physics, University of Cologne, 50937 Cologne, Germany
[2]Joint Quantum Institute, University of Maryland, College Park, Maryland 20742, USA

(Received 5 February 2024; revised 5 March 2025; accepted 29 May 2025; published 7 July 2025)

We construct an observable mixed-state topological order parameter for symmetry-protected free-fermion matter. It resolves the entire table of topological insulators and superconductors, relying exclusively on the symmetry class, but not on unitary symmetries. It provides a robust, quantized signal not only for pure ground states, but also for mixed states in or out of thermal equilibrium. Key ingredient is a unitary probe operator, whose phase can be related to spectral asymmetry, in turn revealing the topological properties of the underlying state. This is demonstrated analytically in the continuum limit, and validated numerically on the lattice. The order parameter is experimentally accessible via either interferometry or full counting statistics, for example, in cold-atom experiments.

DOI: 10.1103/h1qg-96kw

I. INTRODUCTION

Rapid advances in engineered quantum systems, including cold-atomic gases [1–5] or, more broadly, noisy intermediate-scale quantum (NISQ) platforms [6–9], have enabled novel strategies for quantum state preparation, and have unlocked new diagnostic tools for global observables. These platforms provide ideal settings for exploring topological matter, characterized by nonlocal order parameters. However, inevitable interactions with the environment drive them into mixed states, posing challenges beyond the ideal assumption of pure states [10–19] while also creating new opportunities. Consequently, the study of topology in mixed states has emerged as a key focus, with a major challenge posed by the identification of experimentally accessible topological signatures. Among mixed states, fermion Gaussian states represent an important class, whose pure state limit forms the basis of our understanding of topological insulators and superconductors protected by symmetry [10,12,15,16,18,19]. These states arise naturally, for example, from finite-temperature Gibbs ensembles, dissipation engineering [20–22], and synthetic quantum systems [23–26]. Even for spin systems, spin-to-fermion mappings can offer insight into the former [27–30]. The first steps towards identifying and understanding the topological structures of mixed Gaussian states were achieved in specific one- [31] and two-dimensional [32–34] systems in terms of the Uhlmann phase. Complementarily, experimentally relevant observables for Gaussian mixed-state topology have been constructed for models such as the Rice-Mele model, Chern and quantum spin Hall insulators [35–37]. A general experimentally accessible order parameter valid for the entire table of topological insulators and superconductors, and in particular, the identification of an overarching mathematical principle behind it, remains outstanding.

In this paper, we uncover a unified topological order parameter based on symmetry principles, applicable to all Gaussian-state symmetry classes. Our construction requires minimal input, the symmetry class of the stationary state, regardless of its dynamical origin, equilibrium, or nonequilibrium. Its output is universal, connecting the physical signal to the asymmetry matrix Q_W introduced below, a single object which applies across the entire periodic table of topological insulators and superconductors. The order parameter provides a robust, quantized signal, reflecting the topological term in the partition function, and thus distinguishing different topological phases. The resulting mixed-state topological phase represents a direct generalization of the pure state cases in the classic Refs. [15,16]. This unifies pure- and mixed-state systems in a common symmetry-based framework. In addition, it centers on physical observables at the core of the theory: Experimentally, this order parameter can be observed in cold-atom systems, for instance, via interferometry [35,38] or, as we demonstrate here, through full counting statistics of global observables, such as total particle number or spin [39–44]. Thus, our top-down approach renders a systematic recipe for detecting pure- and mixed-state topological phases, moving beyond previous instance-specific proposals for experimental protocols [45,46].

II. A TOPOLOGICAL ORDER PARAMETER FOR ALL SYMMETRY CLASSES

Topology is a nonlocal property of fermions [15,16], and we thus use a global unitary operator as a probe. Its expectation value forms a nonunitary partition function. Its phase, as a topological term [15], yields a topological order parameter. This phase renders a quantized signal due to symmetry, distinguishing different phases. Phase transitions can thus occur

either by breaking the protecting symmetry, or by encountering a zero in the partition function, akin to Lee-Yang zeros. Specifically, we will consider

$$\phi_W[w] = \arg[\mathcal{Z}_W[w]], \quad \mathcal{Z}_W[w] = \langle e^{-i\hat{W}[w]} \rangle,$$
$$\hat{W}[w] = \sum_{i,a,b} \hat{\psi}^\dagger_{i,a} w_i \mathcal{W}_{ab} \hat{\psi}_{i,b}, \tag{1}$$

where $\langle \dots \rangle = \mathrm{Tr}[\hat{\rho} \dots]/\mathrm{Tr}[\hat{\rho}]$, $\hat{\psi}_{i,a}(\hat{\psi}^\dagger_{i,a})$ are the fermionic annihilation (creation) operators at site i with internal indices a. The state of the system is characterized by its density matrix $\hat{\rho} = e^{-\hat{G}}$, taken to be Gaussian, $\hat{G} = \sum_{ij,ab} \hat{\psi}^\dagger_{i,a} G_{ij,ab} \hat{\psi}_{j,b}$: G is local in real space; the topological signal will be activated in the presence of background gauge fields $G = G[A]$. Such density matrix represents gapped fermionic matter in different symmetry classes in [12] and out of equilibrium [21,31–33,37,47,48]. Pure states obtain in zero-temperature ground states ($\hat{G} = \beta\hat{H}$ for inverse temperature β and Hamiltonian $\hat{H}$, in the limit $\beta \to \infty$), or as dark states of Lindbladian evolution [37,48]. The probe operator is characterized by a possibly space-dependent real function w_i, and a Hermitian matrix in internal space $\mathcal{W}$, with the constraint $\mathcal{W}^2 = \mathbb{I}$. We will demonstrate that for a suitable choice of $\mathcal{W}$, the winding of w will activate the topological charge contained in $\hat{G}$, across all classes. This winding features the product of momentum- and real-space topological invariants. The momentum-space topological invariant includes examples like the Chern number. The real-space topology derives from the homotopic characteristics of the background gauge fields within $\hat{G}[A]$. The latter bifurcate into two classes, either U(1) gauge fields for U(1) symmetric insulators, or $\mathbb{Z}_2$ gauge fields for superconductors with fermion parity symmetry. Our focus is on the U(1) case, with the necessary adjustments for $\mathbb{Z}_2$ provided subsequently.

The choice of w is determined exclusively by the spatial dimension:

(1) Even spatial dimensions: w is a spatially homogeneous constant with value $[0,\ 2\pi]$. It spans a parameter cycle, such that $\frac{\Delta\phi_W}{2\pi} \equiv \int_0^{2\pi} \frac{dw}{2\pi} \partial_w \phi_W \in \{\mathbb{Z},\ 2\mathbb{Z},\ \mathbb{Z}_2\}$ renders a phase winding number, detecting the underlying topology.

(2) Odd spatial dimensions: $w = w_i$ is an inhomogeneous function, varying slowly in one spatial direction and constant otherwise, respecting periodic boundary conditions [49]. The order parameter is then $\frac{\phi_W}{\pi}$ itself, i.e., $\frac{\phi_W}{\pi} \in \{\mathbb{Z},\ 2\mathbb{Z},\ \mathbb{Z}_2\}$.

The form of $\mathcal{W}$ is instead determined by symmetry. Symmetry-protected fermion matter falls into two categories [12,19,47,48]: (i) the prime series with integer topological invariant, $\mathbb{Z}$ or $2\mathbb{Z}$ valued; and (ii) the descendant states with $\mathbb{Z}_2$ invariant. The form of $\mathcal{W}$ changes accordingly (see Fig. 1 for an overview):

(1) For the prime series, $\mathcal{W} = \mathbb{I}$.

For the descendant states, a symmetry constraint upon $\mathcal{W}$ is needed:

2(a) For systems without chiral symmetry ["No CS" in Fig. 1(c)], we require that $\mathcal{S}\mathcal{W}\mathcal{S}^{-1} = -\mathcal{W}$, with $\mathcal{S}$ the matrix representation of the protecting time-reversal ($\mathcal{T}$) or particle-hole symmetry ($\mathcal{C}$) [50].

2(b) For systems with chiral symmetry ["CS" in Fig. 1(c)], we require that (a) $\mathcal{W}$ anticommute with chiral symmetry,

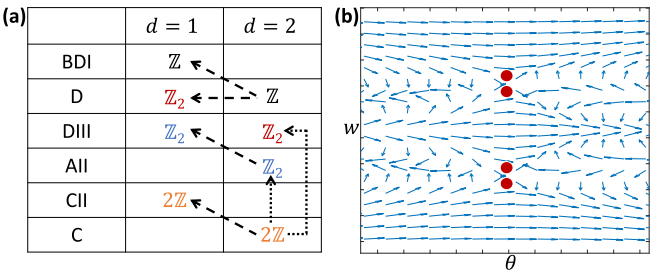

(c)

	ℤ (or 2ℤ) class	ℤ2 class	
		No CS	CS
even d	$\mathcal{W} = \mathbb{I}$ (1) $Q_W \in \mathbb{Z}$ (or $2\mathbb{Z}$) class	$\mathcal{W}$ (2. a) $Q_W \in 2\mathbb{Z}$ class	$\mathcal{W}$ (2. b) $Q_W \in 2\mathbb{Z}$ class

FIG. 1. Mixed-state order parameter concept. (a) In even spatial dimensions ($d = 2$ here), we construct the mixed-state order parameter by choosing the probe matrix $\mathcal{W}$ [Eq. (1)] such that Q_W [Eq. (3)] belongs to the $2\mathbb{Z}$ class, serving as a parent for $\mathbb{Z}_2$ classes (dotted arrows). Results in odd spatial dimensions ($d = 1$ here) are inferred via dimensional reduction (dashed arrows). (b) The reduction to $\mathbb{Z}_2$ arises from an ambiguity in the choice of $\mathcal{W}$: different $\mathcal{W}$ change $\frac{\Delta\phi_W}{2\pi}$ by $4\mathbb{Z}$, manifesting as the appearance of a quartic number of Lee-Yang zeros in the parameter space for the complex amplitude $\mathcal{Z}_W[w]$ [Eq. (1)], where θ parametrizes different $\mathcal{W}$. (c) Overview of the choices of $\mathcal{W}$.

(b) $\mathcal{T}\mathcal{W}\mathcal{T}^{-1} = -\mathcal{W}$ (or $\mathcal{C}\mathcal{W}\mathcal{C}^{-1} = -\mathcal{W}$) in $4k+2$ (or $4k$) spatial dimensions, with $k \in \mathbb{N}_0$.

This will be explained by the $\mathcal{W}$ matrix being inferred from a $2\mathbb{Z}$ class parent in the same dimension [see Fig. 1(a)]. For a fixed $\mathcal{W}$, the ensuing accumulated phase signal consequently satisfies $\frac{\Delta\phi_W}{2\pi} \in 2\mathbb{Z}$. The reduction to $\mathbb{Z}_2$ then arises from the freedom in choosing $\mathcal{W}$ matrices compatible with the above symmetries, demonstrating that the signal is defined only modulo $4\mathbb{Z}$. We take advantage of this mechanism to detect the $\mathbb{Z}_2$ signal $\frac{\Delta\phi_W}{2\pi}$ via random sampling of $\mathcal{W}$.

In this discussion, we have assumed even dimension. For the odd-dimensional cases, the $\mathcal{W}$ matrix can be taken the same as for its even-dimensional parent state, following from dimensional reduction [37,51,52] [see Fig. 1(a)]. We now derive these results, and illustrate them via examples. To this end, we will pass to the continuum limit, where $G_{ij,ab}$ becomes a first-quantized local operator, and w_i a function on d-dimensional space; our results are expected to equally hold on the lattice [53], as confirmed by our numerical simulations.

III. $\Delta\phi_W$ MEASURES ACTIVATED TOPOLOGICAL CHARGE

We focus on Eq. (1), and demonstrate that the winding of w activates quantized topological charge of $\hat{G}$, measured by $\Delta\phi_W$. This will be achieved by identifying $\frac{\Delta\phi_W}{2\pi}$ as a *spectral asymmetry*, which is a topological index [54,55]. Namely, upon tracing out fermion degree of freedom in Eq. (1), one obtains

$$\phi_W = \mathrm{Im}\ \ln\ \det \left\{ \cos\frac{w}{2} + i \sin\left(\frac{w}{2}\right) \left[\mathcal{W} \tanh\left(\frac{G}{2}\right) \right] \right\}. \tag{2}$$

It represents a multivalued function due to the presence of a branch cut in the logarithm [56]. Specifically, upon performing a winding $w \to w + 2\pi$, this multivaluedness singles out the topological charge encapsulated in G, manifesting itself as the spectral asymmetry of the Hermitian *asymmetry matrix* Q_W (see Appendix A),

$$Q_W \equiv \tfrac{1}{2}\{\mathcal{W}, \mathrm{sign}(G)\} \tag{3}$$

with $\mathrm{sign}(G) \equiv \frac{\tanh(\frac{G}{2})}{\sqrt{\tanh(\frac{G}{2})^2}}$ for gapped G, and

$$\frac{\Delta\phi_W}{2\pi} = \frac{1}{2}\sum_n \mathrm{sign}(q_n), \tag{4}$$

with q_n the eigenvalues of Q_W [57]. Here the winding is implemented via spatially homogeneous w, the discussion for slowly varying w is postponed to later. Notably, $\Delta\phi_W$ is β independent ($G = \beta H$) and well defined for any $\beta \neq 0$. Thus, the topological phase structure in the Gaussian pure-state limit is matched by our order-parameter approach. We also note that in interacting systems a transition can happen at finite β, as exemplified in Ref. [58].

According to Atiyah, Patodi, and Singer [54,55], the spectral asymmetry of an elliptic (local) Hermitian operator is related to topology. Here, this manifests as the product of momentum- (denoted as ch_W) and real-space ($\int \mathfrak{C}$) topological invariants,

$$\frac{\Delta\phi_W}{2\pi} = \mathrm{ch}_W \int d^d\boldsymbol{x}\, \mathfrak{C}(\boldsymbol{x}) \in \mathbb{Z}, \tag{5}$$

which is the fundamental formula for our mixed-state order parameter. Specifically, ch_W captures the topological properties of Q_W, characterized by the homotopy group, e.g., $\pi_{d+1}[\mathrm{GL}(N, \mathbb{C})]$ for the map from frequency-momentum space (with dimension $d+1$) to $\frac{1}{i\omega - Q_W} \in \mathrm{GL}(N, \mathbb{C})$. Clearly, for $\mathcal{W} = \mathbb{I}$, this reproduces the Chern number in the Chern insulator. Meanwhile, $\int \mathfrak{C}$ depends only on homotopic properties of the background field, with $\mathfrak{C}$ for the associated topological charge density [59]. For the case of U(1) gauge fields A and in even spatial dimensions $d = 2n$, $\int \mathfrak{C}$ can be the background topological charge of a magnetic field, or the winding number of skyrmions [60],

$$\mathfrak{C}^{(2n)}(\boldsymbol{x}) = \frac{\epsilon^{0i_1i_2\ldots i_{2n-1}i_{2n}}}{(2\pi)^n n!}\partial_{i_1}A_{i_2}\ldots\partial_{i_{2n-1}}A_{i_{2n}}. \tag{6}$$

Together, $\frac{\Delta\phi_W}{2\pi}$ captures the topological charge localized within real-space solitons [61,62], underpinning its role as an order parameter of mixed-state topology.

The spectral asymmetry $\frac{\Delta\phi_W}{2\pi}$ closely links to the fermion parity expectation value, but crucially provides a finer resolution. Specifically, the bridging formula is

$$\mathrm{sign}\langle(-1)^{\hat{Q}}\rangle = e^{i\pi\times(\frac{\Delta\phi_W}{2\pi})}, \tag{7}$$

established by recognizing that $e^{i\phi_W}|_{w=\pi}$ coincides with the fermion parity, as a consequence of $\mathcal{W}^2 = \mathbb{I}$. Meanwhile, Hermiticity of $\mathcal{W}$ implies that $\phi_W(w) = -\phi_W(-w)$, and thus both $e^{i\phi_W}|_{w=\pi}$ and the fermion parity discern only even or oddness of $\frac{\Delta\phi_W}{2\pi}$, yielding a $\mathbb{Z}_2$ signature. The $\mathbb{Z}$-valued spectral asymmetry $\frac{\Delta\phi_W}{2\pi}$ instead captures a richer topological pattern.

Changes in $\frac{\Delta\phi_W}{2\pi}$ can only occur when Q_W contains zero modes. This implies the appearance of Lee-Yang zeros in $\mathcal{Z}_W$, which can be viewed as a nonunitary partition function. These fall into two categories. Indeed, the existence of a Lee-Yang zero is a sufficient, but not a necessary condition for a topological phase transition: The latter occurs for zero modes of G (which implies zero modes of Q_W). But zero modes of Q_W can also occur while G remains gapped, depending on the choice of $\mathcal{W}$ matrices. Symmetry [points 1 and 2] imposes constraints, ensuring zeros of this type to appear in multiples of four [see Fig. 1(b)] (see Appendix C). This results in a $\mathbb{Z}_2$ classification descending from the $2\mathbb{Z}$-valued $\Delta\phi_W$, as we explain next.

IV. EXHAUSTING ALL SYMMETRY CLASSES BY CHOICE OF $\mathcal{W}$

We now construct $\mathcal{W}$ for all symmetry classes, and thus derive the conditions presented in points 1, 1, and 2 based on the spectral asymmetry formula (5). The real-space topology $\mathfrak{C}$ stems from a U(1) gauge field [see Eq. (6)] for insulators [represented by complex fermions, (i) and (ii) below], and $\mathbb{Z}_2$ gauge fields for superconductors [Majorana fermions, (iii)].

(i) *Insulators in even spatial dimensions.* For the $\mathbb{Z}$ and $2\mathbb{Z}$ classes, the choice is simple: we take $\mathcal{W} = \mathbb{I}$ (cf. [1]), yielding $\frac{\Delta\phi_W}{2\pi} \in \mathbb{Z}$ (or $2\mathbb{Z}$) as mixed-state order parameter. This is possible since these classes possess a nontrivial homotopic invariant $\pi_{d+1}[\mathrm{GL}(N, \mathbb{C})]$ [37,57,63]; the $2\mathbb{Z}$ classification results from the presence of time-reversal and particle-hole symmetries requiring the appearance of an even number of $\mathbb{Z}$-class copies [12].

The $\mathbb{Z}_2$ classes, however, generally render a vanishing signal $\frac{\Delta\phi_W}{2\pi}$ when $\mathcal{W} = \mathbb{I}$ [and thus positive fermion parity, cf. Eq. (7)]. This is because symmetry enforces the spectrum of $\mathrm{sign}(G)$ to be composed of symmetric pairs of eigenvalues with opposite sign in Eq. (4) (see Appendix C for details). We thus opt for a different choice of the $\mathcal{W}$ matrix, as listed in points 1 and 2, which endows an opposite sign to the eigenvalues of the symmetric pairs of $\mathrm{sign}(G)$. Namely, we first observe that the associated Q_W is in the $2\mathbb{Z}$ class: Its spectral asymmetry takes values $\frac{\Delta\phi_W}{2\pi} \in 2\mathbb{Z}$, ensured by the positive fermion parity noted above. The reduction to $\mathbb{Z}_2$ then roots in the remaining freedom for choosing $\mathcal{W}$ (see Appendix C): varying $\mathcal{W}$ alters $\frac{\Delta\phi_W}{2\pi}$ by $4\mathbb{Z}$, manifesting in $\mathcal{Z}_W$ as a multiple of four for the number of Lee-Yang zeros in the parameter plane [see Fig. 1(b)]. Hence, we identify $\mathbb{Z}_2 = 2\mathbb{Z} \mod 4$, and obtain $\frac{\Delta\phi_W}{2\pi} = 0,\ 2 \mod 4$ as a mixed-state order parameter.

(ii) *Insulators in odd spatial dimensions.* For the order parameters in odd spatial dimension, a caveat associated with Eq. (5) is that ch_W generally vanishes, due to Bott periodicity (see, e.g., [64]). Still, one can access the underlying topology by invoking slowly varying $w(\boldsymbol{x})$ [cf. 2], and then establish an order parameter via dimensional reduction [12,63]. We start from a generalization of ϕ_W in Eq. (2) to such $w(\boldsymbol{x})$ (Appendix B for a derivation from a Dirac model):

$$\phi_W \equiv \mathrm{ch}_W \int d^{2n}\boldsymbol{x}\, \mathcal{I}_W[w(\boldsymbol{x})] \times \mathfrak{C}^{(2n)}(\boldsymbol{x}), \tag{8}$$

where $\mathfrak{C}^{(2n)}$ is given in Eq. (6). $\mathcal{I}_W[w(\boldsymbol{x})]$ is a model-dependent multivalued function with the key property

$\mathcal{I}_W|_w^{w+2\pi} = 2\pi$, to uphold the spectral asymmetry [Eq. (5)], i.e., $\frac{\phi_W|_{w=0}^{w=2\pi}}{2\pi} \in \mathbb{Z}$. We can then infer the descendant formula via integrating out one spatial dimension [12,63]. The ensuing odd-dimensional signal, with $\mathcal{W}$ read off from its parent state and inhomogeneous w [see Figs. 1(a) and 1(b), in direction $\boldsymbol{x}_\alpha$] is (see Appendix D)

$$\frac{\phi_W}{\pi} = \mathrm{ch}_W\left(\oint d\boldsymbol{x}_\alpha \frac{\partial}{\partial \boldsymbol{x}_\alpha}\mathcal{I}_W\right)\left[\frac{1}{2\pi}\int d^{2n-2}\boldsymbol{x}\mathfrak{C}^{(2n-2)}\right] \in \mathbb{Z}. \tag{9}$$

This establishes $\frac{\phi_W}{\pi}$ as an order parameter in 2.

(iii) *Superconductors.* Thus far, our focus has been on insulators, i.e., systems with a conserved particle number. This allows us to introduce a U(1) gauge field as a means to activate the spectral asymmetry. While a continuous symmetry is crucial for constructing U(1) gauge fields, it is irrelevant for the definition of symmetry classes [10,65]. Indeed, in the case of particle-hole symmetric fermion matter, representing superconductors, the continuous U(1) symmetry is reduced to a discrete $\mathbb{Z}_2$ fermion parity symmetry. The central concept, spectral asymmetry, remains applicable, but is leveraged in a different manner: it is activated by a $\mathbb{Z}_2$ fermion parity symmetry gauge field instead, implemented through twisted spatial boundary conditions [66]. Hence, our recipe in 1, 1, and 2 generalizes to superconductors. We relegate the details to Appendix G, but illustrate its working in Example II below. In the following we will illustrate our findings with concrete examples with $\mathbb{Z}_2$ classification. The signal can be distilled by randomly and repeatedly choosing the probe matrix $\mathcal{W}$, while respecting the symmetry constraints. We will present results for equilibrium states $G = \beta H$ only; nonequilibrium states including dynamical scenarios are discussed in Appendix E.

V. EXAMPLES

A. Example I: Two-dimensional AII class

We focus on the (modified) Bernevig-Hughes-Zhang model (mBHZ) [67]

$$H = \begin{pmatrix} H_0(\boldsymbol{k}) & -i\Delta\tau^y \\ i\Delta\tau^y & H_0^*(-\boldsymbol{k}) \end{pmatrix}, \quad \mathcal{T} = \sigma^y \otimes \tau^0 \mathcal{K}, \tag{10}$$

with $\tau^{x,y,z}$ (τ^0) for Pauli (unit) matrices, and $\boldsymbol{k}$ for momentum. $H_0 = \boldsymbol{d}\cdot\boldsymbol{\tau}$ with $\boldsymbol{d} = [\sin(k_x),\ \sin(k_y),\ m + \cos(k_x) + \cos(k_y)]$, and the Δ term is introduced to break the z-axis spin rotational symmetry.

Possible choices for the probe matrix compliant with 1 are then $\mathcal{W} = \{\boldsymbol{\sigma}\otimes\tau^{x,\,z,\,0},\ \sigma^0\otimes\tau^y\}$. Numerical results are presented in Fig. 2. The mixed-state topological order parameter accurately reconstructs the zero-temperature phase boundary (red line) from a finite-temperature situation ($\beta = 1$ here).

The topological order parameter can be observed in cold-atom experiments by taking simultaneous snapshots of all particles [40–43], to build the full counting statistics (FCS) of the global operator $\hat{W}$. The FCS signal is the distribution function for the eigenvalues $\overline{W}$ of $\hat{W}[w \equiv 1]$ with w taken to be constant 1, represented as

$$P[\overline{W}] \equiv \langle\delta(\hat{W}[1] - \overline{W})\rangle = \int_0^{2\pi} dw\, e^{iw\overline{W}}\langle e^{-iw\hat{W}[1]}\rangle.$$

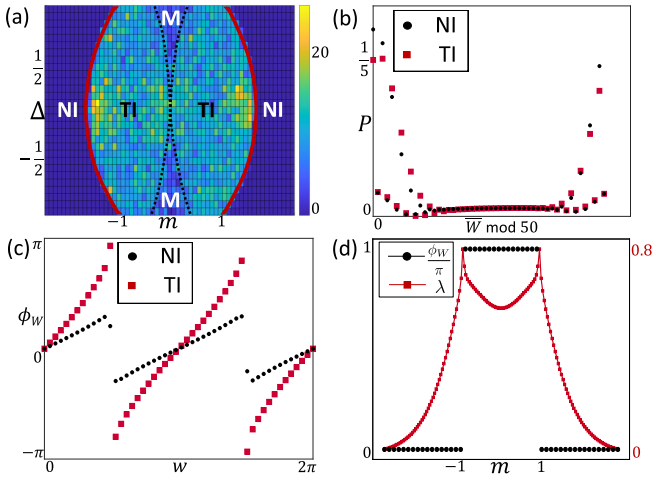

FIG. 2. Numerical results for the modified BHZ (mBHZ) model (a)–(c), and the DIII superconductor (d). (a) $\frac{\Delta\phi_W}{2\pi}$ as a signature for the topological (normal) phase in the mBHZ model under insertion of one magnetic flux quantum at temperature 1 and site number 15×15. $\mathcal{W}$ is randomly sampled 50 times. The color bar is a histogram counting the number of nontrivial valued $\frac{\Delta\phi_W}{2\pi}$, i.e., $\frac{\Delta\phi_W}{2\pi} = 2 \mod 4$ [68]. TI, NI, and M stand for topological, normal, and gapless phase, respectively. (b) Full counting statistics for the mBHZ model in the canonical ensemble at $\beta = 3$, with fixed $\mathcal{W} = \sigma^z\otimes\tau^0$. Its Fourier components encode the mixed-state order parameter ϕ_W, which are plotted in (c), as a function of w, leading to a nontrivial value $\frac{\Delta\phi_W}{2\pi} = 2 \in 2\mathbb{Z} \mod 4$ in TI. (d) Mixed-state topological order parameter for a DIII superconductor as a function of m, i.e., $\frac{\phi_W}{\pi} = \frac{1}{2}\times(0,\ 2 \mod 4)$, where $w = \frac{2\pi x_1}{N_1}$ and $\frac{1}{2}$ from the Majorana nature. The amplitude $\lambda \equiv -\frac{\ln|\mathcal{Z}_W|^2}{N_1}$ exhibits a cusp at the transition points.

Its Fourier components at frequency w render the mixed-state order parameter $\mathcal{Z}_W[w]$. Results for representative points in the normal (NI) and topological (TI) phases are shown in Figs. 2(b) and 2(c): While the FCS histogram looks qualitatively similar in both phases, the topologically nontrivial character is clearly visible in TI, indicated by the winding number along tuning w. Alternatively, Mach-Zehnder interferometry could be used [35,36,38], where $\hat{W}$ acts as the Hamiltonian for an adiabatically imprinted Loschmidt echo [69–72]. This requires immersing the atoms in a cavity, and engineering a probe Hamiltonian defined with w and $\hat{W}$.

B. Example II: One-dimensional DIII class

To illustrate the dimensional reduction method and the Majorana case, we consider the DIII class superconductor in one dimension. Its parent class is AII in two dimensions. Numerical results are shown in Fig. 2(d) for the following model:

$$H = -(\sin k_x\sigma^z)\otimes\tau^x + (m + \cos k_x)\sigma^0\otimes\tau^z, \tag{11}$$

in the Nambu basis $\hat{\Psi}_k = (\hat{\psi}_k,\ -i\sigma^y\hat{\psi}_k^\dagger)$. According to point 1, we choose time-reversal odd probe matrices, realized by the Pauli matrices, i.e., $\mathcal{W} = \boldsymbol{n}\cdot\boldsymbol{\sigma}$ (or $\frac{1}{2}\boldsymbol{n}\cdot\boldsymbol{\sigma}\otimes\tau^0$ in Nambu space) for a spin pointing in direction $\boldsymbol{n} = (\sin\theta\cos\phi,\ \sin\theta\sin\phi,\ \cos\theta)$, and sample the angles

randomly. Figure 2(d) verifies our order parameter as a probe of the underlying topology.

VI. CONCLUSION

We define mixed-state topological phases via topological order parameters, which complements the two-way quantum channel connectivity definition [73], offering clear operational meaning and experimental accessibility. At the heart of the possibility of exhausting the full periodic table with a single topological order parameter lies a new descendant relation between the $2\mathbb{Z}$ and $\mathbb{Z}_2$ classes in the same dimension. While concentrating on free fermions here, the order parameter remains well defined (with the same bilinear $\hat{W}$) for interacting fermion systems. Their mixed-state physics might be enriched by the activation of defects and novel entropy driven topological phase transitions [58]. A further direction is to connect the symmetry-protected topology of mixed fermion states to topological order and the robustness of quantum information [74–78], where mixed Gaussian fermion states can provide a powerful building block [30].

ACKNOWLEDGMENTS

The authors wish to thank X.-Q. Sun for his valuable contributions in the initial phase of this research, especially for suggesting the random sampling numerics of $\mathcal{W}$. We also wish to acknowledge F. Meinert for discussions, and L. Zhao for his insights regarding the index theorem on a lattice. Z.-M.H. acknowledges the support from the JQI postdoctoral fellowship at the University of Maryland. S.D. is supported by the Deutsche Forschungsgemeinschaft (DFG, German Research Foundation) under Germany's Excellence Strategy Cluster of Excellence Matter and Light for Quantum Computing (ML4Q) Grant No. EXC 2004/1 390534769 and by the DFG Collaborative Research Center (CRC) 183 Project No. 277101999-project B02.

APPENDIX A: $\frac{\Delta\phi_W}{2\pi}$ CAN CHANGE ONLY WHEN Q_W IS GAPLESS

We demonstrate that for a fermionic Gaussian state $\hat{\rho}=e^{-\hat{\psi}^\dagger G\hat{\psi}}$, $\frac{\Delta\phi_W}{2\pi}$ depends only on the spectral asymmetry of Q_W, providing the details for the derivation of Eq. (2).

1. Tracing out fermion degree of freedom

We first trace out fermion degree of freedom to reproduce Eq. (2) in the main text. For concreteness, we shall assume $\hat{\psi}$ to be complex fermion, while derivations for the Majorana case (or fermions in the Nambu space) are parallel, as we shall comment along the way. The object of interest is

$$\phi_W(w)\equiv \arg\left[\frac{1}{\mathrm{Tr}\hat{\rho}}\mathrm{Tr}(\hat{\rho}e^{-iw\hat{\psi}^\dagger\mathcal{W}\hat{\psi}})\right],\quad \hat{\rho}=e^{-\hat{\psi}^\dagger G\hat{\psi}}, \tag{A1}$$

which after tracing out fermions, yields

$$\begin{aligned}\phi_W(w)&=\arg\left[\frac{\det(\mathbb{I}+e^{-G}e^{-iw\mathcal{W}})}{\det(1+e^{-G})}\right]\\&=\arg\left[\det(e^{-i\frac{w}{2}\mathcal{W}})\frac{\det(e^{i\frac{w}{2}\mathcal{W}}+e^{-i\frac{w}{2}\mathcal{W}}e^{-G})}{\det(1+e^{-G})}\right]\\&=-\frac{w}{2}\mathrm{tr}\mathcal{W}\\&\quad+\arg\left\{\det\left[\cos\left(\frac{w}{2}\right)+i\,\sin\frac{w}{2}\mathcal{W}\,\tanh\left(\frac{G}{2}\right)\right]\right\}.\end{aligned} \tag{A2}$$

Here, we have used the following identity for complex fermion:

$$\mathrm{Tr}(e^{-\hat{\psi}^\dagger A\hat{\psi}}e^{-\hat{\psi}^\dagger B\hat{\psi}})=\det\left(\mathbb{I}+e^{-A}e^{-B}\right), \tag{A3}$$

while its counterpart for Majorana fermions $\hat{\gamma}$ is [79]

$$[\mathrm{Tr}(e^{-\hat{\gamma}A\hat{\gamma}}e^{-\hat{\gamma}B\hat{\gamma}})]^2=\det(\mathbb{I}+e^{-2A}e^{-2B}). \tag{A4}$$

2. $\frac{\Delta\phi_W}{2\pi}$ as the spectral asymmetry of Q_W

Now we demonstrate one of our key results, that $\frac{\Delta\phi_W}{2\pi}$ only depends on the spectral asymmetry of the Hermitian matrix

$$Q_W=\frac{1}{2}\left\{\mathcal{W},\frac{\tanh\left(\frac{G}{2}\right)}{\sqrt{\tanh^2\left(\frac{G}{2}\right)}}\right\}. \tag{A5}$$

Hence, $\Delta\phi_W$ can change only when the gap of Q_W closes.

The proof is based on the following two observations:

(1) Due to Hermiticity of $\mathcal{W}$:

$$\begin{aligned}\phi_W(w)&=-\phi_W(-w)\Rightarrow\Delta\phi_W\\&=2\int_0^\pi dw\,\partial_w\phi_W(w)=2\phi(\pi),\end{aligned} \tag{A6}$$

which holds since $\phi(0)=0$ [cf. Eq. (A2)].

(2) $\phi_W(w=\pi)$ depends solely on the spectral asymmetry of Q_W.

To demonstrate observation 2, we first use observation 1 and the explicit form of $\phi(\pi)$ [Eq. (A2)] to get

$$\begin{aligned}\Delta\phi_W&=2\,\mathrm{Im}\,\mathrm{Tr}\,\ln\left[i\mathcal{W}\,\tanh\left(\frac{G}{2}\right)\right]\\&=2\,\mathrm{Im}\,\mathrm{Tr}\,\ln\left[i\mathcal{W}\frac{\tanh\left(\frac{G}{2}\right)}{\sqrt{\tanh^2\left(\frac{G}{2}\right)}}\sqrt{\tanh^2\left(\frac{G}{2}\right)}\right]\\&=2\,\mathrm{Im}\,\mathrm{Tr}\,\ln\left[i\mathcal{W}\,\mathrm{sign}(G)\right],\end{aligned} \tag{A7}$$

with

$$\mathrm{sign}(G)\equiv\frac{\tanh\left(\frac{G}{2}\right)}{\sqrt{\tanh^2\left(\frac{G}{2}\right)}} \tag{A8}$$

for gapped G. For gapless G, we notice that the amplitude of ϕ_W vanishes [see Eq. (A2)], so without loss of generality, we extend $\mathrm{sign}(G)$ to encompass the gapless scenario by defining $\mathrm{sign}(0)=0$ in the eigenbasis of G. Here, $i\mathcal{W}\,\mathrm{sign}(G)$ is a unitary matrix, and $\sqrt{\tanh^2(\frac{G}{2})}$ a positive-definite matrix. The proof of Eq. (A7) is delivered below. Hence, by taking the branch cut of the logarithm function on $[-\infty,0]$, we find

$$\frac{\Delta\phi_W}{2\pi}=\frac{1}{\pi}\mathrm{Im}\,\mathrm{Tr}\,\ln\left[i\mathcal{W}\,\mathrm{sign}(G)\right]=\frac{1}{2}\sum_n\mathrm{sign}(q_n), \tag{A9}$$

with q_n eigenvalue for Q_W. The second equality is based on the observation that the formula

$$\mathrm{Im}\int_0^{2\pi}\frac{dx}{2\pi}\partial_x \ln\left(\cos\frac{x}{2}+i\,\sin\frac{x}{2}\lambda\right)=\frac{1}{2}\mathrm{sign}(\mathrm{Re}\lambda), \quad \text{(A10)}$$

for $\lambda\in\mathbb{C}$, singles out the real part of λ. Hence, together with Eqs. (A6) and (A7), we connect ϕ_W with the real part of the eigenvalues of $\mathcal{W}\,\mathrm{sign}(G)$ (recall that this matrix is normal, i.e., unitarily diagonalizable). But the real part of these eigenvalues coincides with the eigenvalues of $Q_W\equiv\frac{1}{2}\{\mathcal{W},\ \mathrm{sign}(G)\}$, which holds since $\mathcal{W}\,\mathrm{sign}(G)$ and $\mathrm{sign}(G)\mathcal{W}=[\mathcal{W}\,\mathrm{sign}(G)]^\dagger$ are diagonalized by the same unitary transformation. Using the interpolation $\mathrm{Im\,Tr\,ln}[\cos(\frac{x}{2})+i\,\sin(\frac{x}{2})\mathcal{W}\,\mathrm{sign}(G)]$ between 0 and $\frac{1}{\pi}\mathrm{Im\,Tr\,ln}[i\mathcal{W}\,\mathrm{sign}(G)]$, Eq. (A9) follows.

Proof of Eq. (A7). It is based on the defining properties of the matrix logarithm and the Baker-Campbell-Hausdorff formula. For notational simplicity, we rewrite it as

$$\mathrm{Im\,Tr\ ln}\,(U\times A)\stackrel{?}{=}\mathrm{Im\,Tr\ ln}\,U, \quad \text{(A11)}$$

where U an unitary matrix and A a positive-definite matrix. By definition of the matrix logarithm, we have

$$U=e^{\ln U},\quad A=e^{\ln A}. \quad \text{(A12)}$$

Due to the Baker-Campbell-Hausdorff formula $e^{B_1}e^{B_2}=e^{B_1+B_2+[B_1,\ [B_1,\ldots]]}$, we find

$$\begin{aligned}\mathrm{Tr\ ln}\,(U\times A)&=\mathrm{Tr\ ln}\,e^{\ln U+\ln A+[\ln U,\ [\ln U,\ldots]]}\\&=\mathrm{Tr}(\ln U+\ln A),\end{aligned} \quad \text{(A13)}$$

and thus demonstrate Eq. (A11).

APPENDIX B: ACTION (8) FROM DIRAC MODEL

We present a detailed derivation of Eq. (8) from a microscopic Dirac model in the presence of an external U(1) gauge field, for the $\mathbb{Z}_2$ class (see [37] for the $\mathbb{Z}$ or $2\mathbb{Z}$ classes). For concreteness, we present the derivation in $d=2$, the generalization to higher dimension is straightforward. We start from the following continuum model:

$$\hat{G}=\hat{G}_0+\int d^2\boldsymbol{x}[m\hat{\psi}^\dagger(\boldsymbol{x})\sigma^z\otimes(\boldsymbol{n}\cdot\boldsymbol{\tau})\hat{\psi}(\boldsymbol{x})] \quad \text{(B1)}$$

and

$$\begin{aligned}\hat{G}_0=\int d^2\boldsymbol{x}\,\hat{\psi}^\dagger(\boldsymbol{x})[&(i\partial_x-A_x)\sigma^x\otimes\tau^0\\&+(i\partial_y-A_y)\sigma^y\otimes\tau^0]\hat{\psi}(\boldsymbol{x}),\end{aligned} \quad \text{(B2)}$$

where $\boldsymbol{n}$ is a unit vector, and $\boldsymbol{x}$ the two-dimensional spatial coordinate. We will reserve the symbol G_0 (G) for the first-quantized counterparts of $\hat{G}_0$ ($\hat{G}$), i.e.,

$$G_0\equiv[i\partial_x-A_x(\boldsymbol{x})]\sigma^x\otimes\tau^0+[i\partial_y-A_y(\boldsymbol{x})]\sigma^y\otimes\tau^0, \quad \text{(B3)}$$

containing two decoupled massless Dirac operators under U(1) gauge field (A_x,A_y), and

$$G=G_0+m\sigma^z\otimes(\boldsymbol{n}\cdot\boldsymbol{\tau}), \quad \text{(B4)}$$

involving a mass term $m\sigma^z\otimes\boldsymbol{n}\cdot\boldsymbol{\tau}$. As for the probe operator, we take $\mathcal{W}=\boldsymbol{s}\cdot\boldsymbol{\tau}\otimes\sigma^0$ with $\boldsymbol{s}$ a unit vector, such that

$$\begin{aligned}\phi_W&\equiv\mathrm{argTr}(e^{-i\int d^2\boldsymbol{x}\,\hat{\psi}^\dagger w\boldsymbol{s}\cdot\boldsymbol{\tau}\otimes\sigma^0\hat{\psi}}e^{-\hat{G}})\\&=\mathrm{Im}\Big\{\mathrm{Tr\ ln}\,e^{-i\frac{1}{2}w\boldsymbol{s}\cdot\boldsymbol{\tau}\otimes\sigma^0}\\&\quad+\mathrm{Tr\ ln}\left[\cos\left(\frac{w}{2}\right)+i\,\sin\left(\frac{w}{2}\right)\boldsymbol{s}\cdot\boldsymbol{\tau}\otimes\sigma^0\tanh\left(\frac{G}{2}\right)\right]\Big\},\end{aligned} \quad \text{(B5)}$$

where w is homogeneous, and Tr is for tracing over both the internal and spatial space, while tr is preserved for internal space.

In the rest of this section, we will show that

$$\begin{aligned}\phi_W&=\mathrm{ch}_W\int d^2\boldsymbol{x}\,\mathcal{I}_W[w]\times\mathcal{N},\qquad \mathcal{N}=\frac{1}{2\pi}\epsilon^{ij}\partial_iA_j,\\\mathcal{I}_W[w]&=\mathrm{Re}\Big\{-i\,\mathrm{tr\ ln}\left[\cos\left(\frac{w}{2}\right)\right.\\&\quad\left.+i\,\sin\left(\frac{w}{2}\right)\boldsymbol{s}\cdot\boldsymbol{\tau}\tanh\frac{|m|(\boldsymbol{n}\cdot\boldsymbol{\tau})}{2}\right]\Big\}.\end{aligned} \quad \text{(B6)}$$

with $\mathrm{ch}_W=2\frac{\mathrm{sign}(m)}{2}$. Here, $\mathcal{N}$ is the topological index density of G_0, which in the presence of the external magnetic field equals the specified expression. It counts the number of zero modes associated with G_0. It is interesting to note that all the topological information is contained in G_0, while both the mass term (associated to $\boldsymbol{n}$) and the probe operator (associated to $\boldsymbol{s}$) appear exclusively in the function $\mathcal{I}_W$. The relation between the zero modes of the Dirac operator and the topological index is the content of the Atiyah-Singer index theorem; it holds in higher even space dimensions too, so that analogous results can be derived straightforwardly, inferred from the index theorem.

To proceed, we will represent ϕ_W in the eigenbasis of G_0 (including inhomogeneous external fields), aiming to demonstrate that ϕ_W is only from zero modes of G_0. We first notice that G_0 has the following symmetries:

$$\{G_0,\ \sigma^z\}=0,\qquad [G_0,\ (\boldsymbol{s}\cdot\boldsymbol{\tau}\otimes\sigma^0)]=0, \quad \text{(B7)}$$

from which we infer the following:

(i) Eigenstates of G_0 with *nonzero* eigenvalues appear in opposite eigenvalue pairs, namely $|\psi_n\rangle$, $\sigma^z|\psi_n\rangle$, with eigenvalues $\pm\lambda_n$. For later notational simplicity, we preserve the $n=0$ index for the zero-eigenvalue sector.

(ii) We can diagonalize G_0 and $\boldsymbol{s}\cdot\boldsymbol{\tau}\otimes\sigma^0$ simultaneously, and thus label $|\psi_n\rangle$ by $|\psi_n^\pm\rangle$ for the positive (negative) eigenvalue of $\boldsymbol{s}\cdot\boldsymbol{\tau}$.

Together, the contribution to ϕ_W from the eigenstates $|\psi_n^\pm\rangle$'s ($n\neq0$) is

$$\arg\mathrm{Tr}_n\left[\cos\left(\frac{w}{2}\right)+i\,\sin\left(\frac{w}{2}\right)\boldsymbol{s}\cdot\boldsymbol{\tau}_n\tanh\left(\frac{1}{2}G_n\right)\right], \quad \text{(B8)}$$

where the subscript n is to emphasize the restriction to the subspace spanned by $\{|\psi_n^\pm\rangle,\ \sigma^z|\psi_n^\pm\rangle\}$'s, e.g., Tr_n for tracing

over this subspace, and $\boldsymbol{s}\cdot\boldsymbol{\tau}_n$ and G_n are

$$\boldsymbol{s}\cdot\boldsymbol{\tau}_n \equiv \begin{pmatrix} \begin{pmatrix} 1 & \\ & -1 \end{pmatrix} & 0 \\ 0 & \begin{pmatrix} 1 & \\ & -1 \end{pmatrix} \end{pmatrix} \tag{B9}$$

and

$$G_n \equiv \begin{pmatrix} \lambda_n \mathbb{1} & m\boldsymbol{n}\cdot\boldsymbol{\tau} \\ m\boldsymbol{n}\cdot\boldsymbol{\tau} & -\lambda_n\mathbb{1} \end{pmatrix}. \tag{B10}$$

After these preparations, we are ready to demonstrate that ϕ_W receives no contributions from $n\neq 0$ states, i.e., Eq. (B8) vanishes for $n\neq 0$. This is based on the following two properties: 1. $(\boldsymbol{s}\cdot\boldsymbol{\tau}_n)^2=\mathbb{1}$; 2. G_n possesses chiral symmetry, i.e., $\{G_n, M\}=0$ where $M\equiv\left(\begin{smallmatrix}0 & -i\mathbb{1}\\ i\mathbb{1} & 0\end{smallmatrix}\right)$. In turn, we find $\mathrm{Tr}_n[\cos(\frac{w}{2})+i\sin(\frac{w}{2})\boldsymbol{s}\cdot\boldsymbol{\tau}_n\tanh(\frac{1}{2}G_n)]$ is real, i.e.,

$$\begin{aligned}
&\mathrm{Tr}_n \ln\left[\cos\left(\frac{w}{2}\right)+i\,\sin\left(\frac{w}{2}\right)\boldsymbol{s}\cdot\boldsymbol{\tau_n}\tanh\left(\frac{G_n}{2}\right)\right]\\
&\quad=\mathrm{Tr}_n[M(\boldsymbol{s}\cdot\boldsymbol{\tau}_n)]\ln\left[\cos\left(\frac{w}{2}\right)\right.\\
&\qquad\left.+\,i\sin\left(\frac{w}{2}\right)\tanh\left(\frac{1}{2}G_n\right)\boldsymbol{s}\cdot\boldsymbol{\tau}_n\right][M(\boldsymbol{s}\cdot\boldsymbol{\tau}_n)]^\dagger\\
&\quad=\mathrm{Tr}_n\ln\left[\cos\left(\frac{w}{2}\right)+i\,\sin\left(\frac{w}{2}\right)\boldsymbol{s}\cdot\boldsymbol{\tau}_n\tanh\left(\frac{G_n}{2}\right)\right]^\dagger.
\end{aligned} \tag{B11}$$

Built upon results above, we conclude that ϕ_W is from the $n=0$ state (zero mode of G_0). To finally obtain Eq. (B6), we proceed by utilizing the chiral symmetry of G_0, from which we can take the zero mode to be eigenstates of σ^z, labeled by $\alpha=\pm$. In turn, ϕ_W becomes

$$\begin{aligned}
\phi_W=\sum_{\alpha=\pm}\mathrm{Re}(-i)\mathrm{tr}\,\ln\left[\cos\left(\frac{w}{2}\right)\right.\\
\left.+\,i\,\sin\left(\frac{w}{2}\right)\boldsymbol{s}\cdot\boldsymbol{\tau}\tanh\left(\frac{\alpha m\boldsymbol{n}\cdot\boldsymbol{\tau}}{2}\right)\right],
\end{aligned} \tag{B12}$$

where we have used $[G_0, \boldsymbol{\tau}\otimes\sigma^0]=0$, and here, "tr" is over the two-dimensional $\boldsymbol{\tau}$ matrix. Together with the index theorem, we reproduce Eq. (B6), i.e.,

$$\begin{aligned}
\phi_W&=\mathrm{ch}_W\times(n_{\alpha=+}-n_{\alpha=-})\times\mathcal{I}_W[w]\\
&=\mathrm{ch}_W\times\mathcal{I}_W[w]\times\left(\int\frac{d^2\boldsymbol{x}}{2\pi}\epsilon^{ij}\partial_i A_j\right),
\end{aligned} \tag{B13}$$

with

$$\mathrm{ch}_W=2\,\frac{\mathrm{sign}(m)}{2}\ \text{and}\ n_{\alpha=+}-n_{\alpha=-}\equiv\int d^2\boldsymbol{x}\,\mathcal{N}\in\mathbb{Z}. \tag{B14}$$

In particular, we notice that $\mathcal{I}_W$ satisfies

$$\mathcal{I}_W|_w^{w+2\pi}=\pm 2\pi, \tag{B15}$$

where the $\pm$ originates from the sign of $\mathrm{tr}[(\boldsymbol{s}\cdot\boldsymbol{\tau})\cdot(\boldsymbol{n}\cdot\boldsymbol{\tau})]$. ch_W is the spin Chern number [80–82] for our massive Dirac model: This can be seen clearly in the limit of $\boldsymbol{n}\cdot\boldsymbol{\tau}=\tau^z$, where G consists of two Dirac models with opposite mass, and thus opposite Chern number, i.e., $\pm\frac{1}{2}\mathrm{sign}(m)$ [12]. The half-integer valuedness is attributed to the Dirac model, which can be cured by proper regularization [12,37,83]. These together produce $\mathrm{ch}_W=\frac{1}{2}\mathrm{sign}(m)-[-\frac{1}{2}\mathrm{sign}(m)]=2\frac{\mathrm{sign}(m)}{2}$.

Finally, we highlight that our action is readily generalized to weakly inhomogeneous w, via gradient expansion as derived in [37], by replacing constant w with $w[\boldsymbol{x}]$.

APPENDIX C: $\mathbb{Z}_2$ INVARIANT FROM THE FREEDOM OF CHOOSING $\mathcal{W}$

Here we shall focus on the $\mathbb{Z}_2$ class in even spatial dimensions, and elucidate the emergence of its $\mathbb{Z}_2$ invariant through variation of $\mathcal{W}$. To this end, we shall first demonstrate that opting for the naive choice $\mathcal{W}=\mathbb{I}$ results in a vanishing $\frac{\Delta\phi_W}{2\pi}$. This observation prompts us to seek for an alternative $\mathcal{W}$. We construct it such that the associated Q_W falls in a $2\mathbb{Z}$ class. It turns out that the choice of $\mathcal{W}$ is not unique, which leads to a reduction form $2\mathbb{Z}$ to $\mathbb{Z}_2$ invariant. For concreteness, we shall focus on external U(1) gauge fields in this section.

1. Vanishing $\Delta\phi_W$ for $\mathcal{W}=\mathbb{I}$

We first show that symmetry enforces vanishing $\frac{\Delta\phi_W}{2\pi}|_{\mathcal{W}=\mathbb{I}}=0$ in the $\mathbb{Z}_2$ class in even spatial dimensions. We observe the following:

(i) The periodic table exhibits the following symmetry pattern for the $\mathbb{Z}_2$ classes: In $d=4k$ ($d=4k+2$) spatial dimensions ($k\in\mathbb{Z}$), all the $\mathbb{Z}_2$ classes possess particle-hole (time-reversal) symmetry, i.e., $\mathcal{S}G\mathcal{S}^{-1}=(-1)^{d/2+1}G$, with $\mathcal{S}$ for $\mathcal{C}$ (or $\mathcal{T}$).

(ii) Under an external field with strength tensor $F_{\mu\nu}\equiv\partial_\mu A_\nu-\partial_\nu A_\mu$, the spectral asymmetry formula in Eq. (4) in the main text becomes

$$\frac{\Delta\phi_W}{2\pi}=\mathrm{ch}_W\int\mathfrak{C},\ \text{and}\ \mathfrak{C}=\frac{\epsilon^{0i_1i_2\ldots i_{d-1}i_d}}{(2\pi)^{d/2}(d/2)!}\partial_{i_1}A_{i_2}\ldots\partial_{i_{d-1}}A_{i_d}, \tag{C1}$$

where "$\int$" denotes the integration over the spatial coordinates. Expressed in terms of a magnetic field, we have $\mathfrak{C}=(\frac{B}{2\pi})^{d/2}$.

Consequently, symmetry necessitates vanishing spectral asymmetry: On the one hand,

$$\frac{\Delta\phi_W}{2\pi}=\frac{1}{2}\mathrm{Tr}[\mathrm{sign}(G[A])]=\mathrm{ch}_W\int\mathfrak{C}, \tag{C2}$$

which results from Eq. (A9), by taking $\mathcal{W}=\mathbb{I}$. On the other hand, from time-reversal (particle-hole) symmetry with odd (even) $d/2$,

$$\frac{\Delta\phi_W}{2\pi}=(-1)^{d/2+1}\frac{1}{2}\mathrm{Tr}[\mathcal{S}\,\mathrm{sign}(G[-A])\mathcal{S}^{-1}]=-\mathrm{ch}_W\int\mathfrak{C}, \tag{C3}$$

with $\mathcal{S}=\mathcal{C}$ and $\mathcal{T}$, where for odd $d/2$, the minus sign in the second equality is from $A\to -A$ in $\mathfrak{C}$; for even $d/2$, it is from particle-hole symmetry [$\mathcal{C}G\mathcal{C}^{-1}=(-1)G$], encoded in the prefactor $(-1)^{d/2+1}$. By comparing Eq. (C2) with (C3), we conclude that

$$\frac{\Delta\phi_W}{2\pi}=0. \tag{C4}$$

TABLE I. Symmetry-shifting pattern induced by probe operator: 1. In even spatial dimension: $\mathbb{Z}_2$ and $\mathbb{Z}_2$ to $2\mathbb{Z}$; 2. dimensional reduction, from even spatial dimension to odd spatial dimension: $\mathbb{Z}_2$ (even D) to $\mathbb{Z}_2$ (odd D); $\mathbb{Z}$ (even D) to $\mathbb{Z}_2$ (odd D).

Symmetry class	Symmetry		$d=0$	1	2	3	4	5	6	7	8
AI	$\mathcal{T}^2=1$		$\mathbb{Z}$	0	0	0	$2\mathbb{Z}$	0	$\mathbb{Z}_2$	$\mathbb{Z}_2$	$\mathbb{Z}$
BDI	$\mathcal{T}^2=1$	$\mathcal{C}^2=1$	$\mathbb{Z}_2$	$\mathbb{Z}$	0	0	0	$2\mathbb{Z}$	0	$\mathbb{Z}_2$	$\mathbb{Z}_2$
D		$\mathcal{C}^2=1$	$\mathbb{Z}_2$	$\mathbb{Z}_2$	$\mathbb{Z}$	0	0	0	$2\mathbb{Z}$	0	$\mathbb{Z}_2$
DIII	$\mathcal{T}^2=-1$	$\mathcal{C}^2=1$	0	$\mathbb{Z}_2$	$\mathbb{Z}_2$	$\mathbb{Z}$	0	0	0	$2\mathbb{Z}$	0
AII	$\mathcal{T}^2=-1$		$2\mathbb{Z}$	0	$\mathbb{Z}_2$	$\mathbb{Z}_2$	$\mathbb{Z}$	0	0	0	$2\mathbb{Z}$
CII	$\mathcal{T}^2=-1$	$\mathcal{C}^2=-1$	0	$2\mathbb{Z}$	0	$\mathbb{Z}_2$	$\mathbb{Z}_2$	$\mathbb{Z}$	0	0	0
C		$\mathcal{C}^2=-1$	0	0	$2\mathbb{Z}$	0	$\mathbb{Z}_2$	$\mathbb{Z}_2$	$\mathbb{Z}$	0	0
CI	$\mathcal{T}^2=1$	$\mathcal{C}^2=-1$	0	0	0	$2\mathbb{Z}$	0	$\mathbb{Z}_2$	$\mathbb{Z}_2$	$\mathbb{Z}$	0

Alternatively, the vanishing spectral asymmetry can be attributed to *symmetric pairs*, which is a crucial concept in the following. By a symmetric pair, we refer to two eigenvalues of $\mathrm{sign}(G)$ with opposite sign, whose associated eigenstates are related to each other by a symmetry transformation $\mathcal{S}$. Indeed, imposing of a symmetry compels a pairwise division within the spectrum of G: The symmetry transformation

$$\mathcal{S}G[A]\mathcal{S}^{-1}=(-1)^{d/2+1}G[-A] \tag{C5}$$

implies that for every eigenstate $|\psi[A]\rangle$ with eigenvalue $g[A]$, its symmetric counterpart $\mathcal{S}^{-1}|\psi[-A]\rangle$ has eigenvalue $(-1)^{(d/2+1)}g[-A]$. Thus, the spectrum comprises pairs $\{g[A],\ (-1)^{d/2+1}g[-A]\}$, each with a level degeneracy $|\int\mathfrak{C}|$. Furthermore, motivated by the spectral asymmetry formula (C1), we can restrict our attention to states contributing terms linear in $\int\mathfrak{C}$, whose eigenvalues must satisfy

$$\mathrm{sign}(g[A])=\mathrm{sign}(\mathfrak{C})\Rightarrow \mathrm{sign}(g[A])|\int\mathfrak{C}|=\int\mathfrak{C}, \tag{C6}$$

where $|\int\mathfrak{C}|$ is from level degeneracy, and where we have neglected a possible A-field-independent sign in $g[A]$, as it is irrelevant for our results. Consequently, eigenvalues from these symmetric pairs must exhibit opposite signs, i.e.,

$$\mathrm{sign}\{g[A]\times(-1)^{d/2+1}g[-A]\}=\mathrm{sign}[(-1)^{d+1}]<0, \tag{C7}$$

from which we conclude that the external field activated spectral asymmetry vanishes, due to the presence of symmetric pairs with opposite sign eigenvalues.

So far, we have shown that symmetry enforces symmetric pairs, and thus a vanishing spectral asymmetry (for $\mathcal{W}=\mathbb{I}$), due to a cancellation effect. To cure this problem, i.e., to obtain a finite signal quantitatively probing the underlying topology, our strategy is to reverse the relative sign for these symmetric pairs, implemented via introducing a $\mathcal{W}$ matrix such that $Q_W\equiv\frac{1}{2}\{\mathrm{sign}(G),\ \mathcal{W}\}$ contains nonzero spectral asymmetry, and belongs to the $2\mathbb{Z}$ class.

2. Symmetry constraints for $\mathcal{W}$

To place Q_W in the $2\mathbb{Z}$ class in the same dimension (brown in Table I), possessing an even-integer-valued spectral asymmetry (with $\mathcal{W}=\mathbb{I}$), we equip $\mathcal{W}$ with a symmetry

(1) G without chiral symmetry (blue in Table I): for G with $\mathcal{T}$ (or $\mathcal{C}$) symmetry, $\mathcal{T}\mathcal{W}\mathcal{T}^{-1}=-\mathcal{W}$ (or $\mathcal{C}\mathcal{W}\mathcal{C}^{-1}=-\mathcal{W}$).

To see this, we note that the symmetries of Q_W are

$$\begin{cases}\mathcal{T}G\mathcal{T}^{-1}=G,\\ \mathcal{T}=U_T\mathcal{K},\ \mathcal{T}^2=\pm1,\end{cases}\rightarrow\begin{cases}\mathcal{C}_W Q_W\mathcal{C}_W^{-1}=-Q_W,\\ \mathcal{C}_W=U_T\mathcal{K},\ \mathcal{C}_W^2=\pm1\end{cases} \tag{C8}$$

and

$$\begin{cases}\mathcal{C}G\mathcal{C}^{-1}=-G,\\ \mathcal{C}=U_C\mathcal{K},\ \mathcal{C}^2=\pm1,\end{cases}\rightarrow\begin{cases}\mathcal{T}_W Q_W\mathcal{T}_W^{-1}=Q_W,\\ \mathcal{T}_W=\mathrm{sign}(G)U_C\mathcal{K},\ \mathcal{T}_W^2=\mp1\end{cases}. \tag{C9}$$

which confirms that Q_W belongs to the $2\mathbb{Z}$ class. The property $\mathcal{T}_W^2=\mp1$ in the second equation results from a special symmetry:

$$\begin{aligned}&[Q_W,\ \mathrm{sign}(G)]=0\\ &\quad\Rightarrow\mathcal{T}_W^2=\mathrm{sign}(G)U_C\mathcal{K}\mathrm{sign}(G)U_C\mathcal{K}=-(U_C\mathcal{K})^2\end{aligned} \tag{C10}$$

and, due to this symmetry, the inherited $\mathcal{T}_W$ symmetry can satisfy either $\mathcal{T}_W^2=+1,\ -1$ by dressing up with $\mathrm{sign}(G)$, i.e., $\mathrm{sign}GU_C\mathcal{K}$, and our choice here is to ensure Q_W in the $2\mathbb{Z}$ class. Interestingly, this exhibits a shifting pattern, i.e., $\mathcal{T}(\mathcal{C})\rightarrow\mathcal{C}_W(\mathcal{T}_W)$, which will be utilized to construct the $\mathcal{W}$ matrix for the chiral symmetry $\mathbb{Z}_2$ class, discussed below.

(2) G with chiral symmetry (purple in Table I): (a) $\mathcal{W}$ anticommutes with the chiral symmetry generator;

(b) $\mathcal{T}\mathcal{W}\mathcal{T}^{-1}=-\mathcal{W}$ (or $\mathcal{C}\mathcal{W}\mathcal{C}^{-1}=-\mathcal{W}$) in $4k+2$ (or $4k$) spatial dimensions, with $k\in\mathbb{Z}$.

We focus on the chiral symmetric $\mathbb{Z}_2$ class in even spatial dimensions (blue in Table I). To this end, we observe that they possess both particle-hole and time-reversal symmetry, while the $2\mathbb{Z}$ class in the same dimension (brown in Table I) exhibits either particle-hole or time-reversal symmetry. To bridge this discrepancy, we require $\mathcal{W}$ to anticommute with the chiral symmetry generator [(a) in point 1 above], such that the resulting Q_W is not chiral symmetric. Adding to this, we require Q_W to share the same symmetry as the $2\mathbb{Z}$ class, from which one can straightforwardly infer (b) in point 1 above, via the symmetry-shifting pattern [i.e., $\mathcal{T}(\mathcal{C})\rightarrow\mathcal{C}_W(\mathcal{T}_W)$].

Finally, we outline the construction of $\mathcal{W}$ matrix in odd spatial dimensions, but postpone the details to the later Appendix D, where a parallel scenario unfolds for the $\mathbb{Z}_2$ classes:

(i) For the nonchiral symmetric $\mathbb{Z}_2$ class (purple $\mathbb{Z}_2$ in Table I), $\mathcal{W}=\mathbb{I}$ as ϕ_W can be nonzero.

(ii) For the chiral symmetric class (blue $\mathbb{Z}_2$ in Table I), symmetry dictates vanishing ϕ_W, necessitating an alternative

TABLE II. Changes of $\frac{\Delta\phi_W}{2\pi}$ from transferring symmetric pairs. Q_W contains $2s$ states. *Before* crossing zeros, the number of states in $Q_W^{(1,\pm)}$ (and $Q_W^{(2,\pm)}$) is $r \in \mathbb{Z}$. *After* crossing, the number of states in $Q_W^{(1,+)}$ becomes $r+t \in \mathbb{Z}$. Consequently, the difference in the spectral asymmetry is $2t \in 2\mathbb{Z}$.

Gapless G	$Q_W^{(1,+)}$	$Q_W^{(2,+)}$	$Q_W^{(1,-)}$	$Q_W^{(2,-)}$	$\frac{\Delta\phi_W}{2\pi}$	Changes in $\frac{\Delta\phi_W}{2\pi}$
No. of states (before)	r	r	$s-r$	$s-r$	$2r-s$	$2t \in 2\mathbb{Z}$
No. of states (after)	$r+t$	$r+t$	$s-r-t$	$s-r-t$	$2r-s+2t$	

choice of $\mathcal{W}$ matrix. This is achieved via the method of dimensional reduction, resulting in a $\mathcal{W}$ similar to its even spatial dimensional parent (i.e., blue $\mathbb{Z}_2$ in even spatial dimensions in Table I).

3. $\mathbb{Z}_2$ invariant from the freedom in choosing $\mathcal{W}$

The construction of $\mathcal{W}$ above introduces ambiguities in the selection of $\mathcal{W}$, to be addressed now. The ambiguity is noticed based on the observation that smooth deformations of $\mathcal{W}$ or G lead to *a transfer of symmetric pairs of* sign(G) between the positive and negative eigenvalue sectors of Q_W (denoted as $Q_W^{(\pm)}$), such that a symmetric pair of eigenstates in the $Q_W^{(\pm)}$ subspace is relocated to $Q_W^{(\mp)}$: Here, we have used the property that Q_W commutes with sign(G), so eigenstates associated with a symmetric pair of sign(G) are also eigenstates of Q_W, belonging to the same positive and negative eigenvalue sector of Q_W (see Appendix C 3 a for derivations). From this, we demonstrate the following:

(1) The ensuing change of spectral asymmetry counts twice the number of transferred symmetric pairs.

(2) The condition that G be gapped necessitates an even number of transferred symmetric pairs.

(3) $\mathcal{W}$ and G are independent, so a smooth deformation of $\mathcal{W}$ changes the spectral asymmetry by $4\mathbb{Z}$, from which we establish a $\mathbb{Z}_2 = 2\mathbb{Z} \mod 4$ invariant.

To this end, we first collect properties of Q_W, and introduce notation for later convenience:

(i) $[\text{sign}(G), Q_W] = 0$, so we can diagonalize these two matrices simultaneously, i.e.,

$$Q_W = Q_W^{(1,+)} \oplus Q_W^{(1,-)} \oplus Q_W^{(2,+)} \oplus Q_W^{(2,-)}, \tag{C11}$$

where $\pm$ (or 1, 2) for the positive and negative sign of eigenvalues associated with Q_W [or sign(G)], and $Q_W^{(1/2,\pm)}$ for the subspace consisting of corresponding eigenvectors.

(ii) For notational simplicity, we introduce $\lambda_n^{(1/2,\pm)} = 1$ to enumerate states in the $Q_W^{(1/2,\pm)}$ subspace.

Leveraging the properties listed above and employing Eq. (A9), the spectral asymmetry associated with Q_W is

$$\frac{\Delta\phi_W}{2\pi} = \frac{1}{2}\sum_n \left\{\left[\lambda_n^{(1,+)} + \lambda_n^{(2,+)}\right] - \left[\lambda_n^{(1,-)} + \lambda_n^{(2,-)}\right]\right\}. \tag{C12}$$

Here, $\lambda_n^{(1,+)}$ and $\lambda_n^{(2,+)}$ (as well as $\lambda_n^{(1,-)}$ and $\lambda_n^{(2,-)}$) form a symmetric pair (see Appendix C 3 a for derivation), which ensures that the spectral asymmetry associated with G vanishes, i.e.,

$$\sum_n \left\{\left[\lambda_n^{(1,+)} - \lambda_n^{(2,+)}\right] + \left[\lambda_n^{(1,-)} - \lambda_n^{(2,-)}\right]\right\} = 0. \tag{C13}$$

Now we are ready to establish the $\mathbb{Z}_2$ invariant. To this end, we show that under the constraint that G remain gapped, $\frac{\Delta\phi_W}{2\pi}$ undergoes a change of $4\mathbb{Z}$ under a smooth deformation of $\mathcal{W}$ or G. To achieve this, we first note that the change in spectral asymmetry is equal to twice the number of transferred symmetric pairs, i.e., 1 listed above (see Table II): We assign the number of states in $Q_W^{(1,+)}$ and $Q_W^{(1,-)}$ as $r \in \mathbb{Z}$ and $s-r \in \mathbb{Z}$, respectively, whose ensuing spectral asymmetry is $\frac{\Delta\phi_W}{2\pi} = 2r-s$. After transferring t symmetric pairs between the $Q_W^{(\pm)}$ sectors, i.e., $r \to r+t$ and $s-r \to s-r-t$, the spectral asymmetry changes by $2t \in 2\mathbb{Z}$.

Furthermore, we observe that transferring an odd number of symmetric pairs necessitates a gapless G (i.e., 2 listed above). Illustratively, consider a $\{\lambda_n^{(1/2,+)}\}$ sub-block of G (denoted by $G_{(s)}$), featuring a single symmetric pair, i.e., $G_{(s)} = \xi\tau^z$, where τ^z signifies the symmetric pair with opposite eigenvalues in sign(G). Moreover, $G_{(s)}$ exhibits "particle-hole" symmetry, i.e., $\mathcal{S}_{(s)}G_{(s)}[A]\mathcal{S}_{(s)}^{-1} = -G_{(s)}[A]$ and $\mathcal{S}_{(s)} = \mathcal{K}\tau^x$ (see Appendix C 3 b for a concrete example). This reflects the underlying time-reversal and particle-hole symmetries, enforcing symmetric pairs of sign(G) as elaborated in Appendix C 1. After these preparations, let us implement a smooth deformation. Symmetry $\mathcal{S}_{(s)}$ dictates $\mathcal{W}_{(s)}$ to be $\mathcal{W}_{(s)} = \pm\tau^z$, satisfying $\mathcal{S}_{(s)}\tau^z\mathcal{S}_{(s)}^{-1} = -\tau^z$. Consequently, $Q_{W,(s)} = \text{sign}(\xi)\tau^0$ when $\mathcal{W}_{(s)} = \tau^z$, where sign($\xi$) identifies the belonging to the sectors $Q_W^{(\text{sign}(\xi))}$. Hence, the transfer of a symmetric pair necessitates tuning ξ from positive to negative, closing the gap in G at $\xi = 0$ and inducing a spectral asymmetry change of 2. This underscores the requisite gaplessness in G for symmetric pair transfer.

In contrast, gapped G mandates an even number of transferred pairs (i.e., 3 listed above). Consider an illustrative case of a doublet: $G_{(s)} = \xi\tau^z \otimes \sigma^0$ and $\mathcal{S}_{(s)} = \mathcal{K}\tau^x \otimes \sigma^0$. We transfer this symmetric pair doublet between $Q_W^{\pm}$ through smooth deformations of either $G_{(s)}$ or $\mathcal{W}_{(s)}$, while keeping G gapped. For the former scenario, we deform $G_{(s)}$ by adding an extra mass term allowed by symmetry, i.e., $\tau^y \otimes \sigma^y$, rendering $G_{(s)} = \xi(\cos\theta\tau^z \otimes \sigma^0 + \sin\theta\tau^y \otimes \sigma^y)$, with θ parametrizing the deformation. Taking $\mathcal{W}_{(s)} = \tau^z \otimes \sigma^0$, we find that the asymmetry matrix is $Q_{W,(s)} = \text{sign}(\xi)\cos\theta\tau^0 \otimes \sigma^0$. Thus, a symmetric pair doublet can be transferred by tuning θ, keeping G gapped. Alternatively, the transfer can be achieved by deforming $\mathcal{W}$: Using $G_{(s)} = \xi\tau^z \otimes \sigma^0$ and $\mathcal{W}_{(s)} = \cos\theta\tau^z \otimes \sigma^0 + \sin\theta\tau^y \otimes \sigma^y$, we again infer that $Q_{W,(s)} = \text{sign}(\xi)\cos\theta\tau^z \otimes \tau^0$. Hence, tuning θ enables the transfer of a symmetric pair doublet with G remaining gapped, supporting our earlier assertion.

Together, we conclude that under the constraint of gapped G, the spectral asymmetry changes by $4\mathbb{Z}$, from transferring even number of symmetric pairs. Finally, it is amused

to observe that the even or odd effect of symmetric pairs mirrors the $\mathbb{Z}_2$ classification in zero-dimensional D-class insulators. Specifically, an even number of D-class insulators (e.g., $G_{(s)} = \xi\tau^z$ representing one specific D insulator here), are adiabatically connected with spectral gap open, and thus belongs to the topologically trivial phase.

a. Symmetric pairs of $Q_W^{\pm}$

For sign(G), we have established the existence of eigenvalue pairs with *opposite* signs, linked by symmetry. Extending our investigation to Q_W^+ (Q_W^-), we observe a parallel phenomenon: eigenvalue pairs sharing the *same* sign, interrelated through symmetry, which is referred to as *symmetric pairs of* $Q_W^+(Q_W^-)$. To show this, we adopt a strategy akin to that presented in Appendix C 1, utilizing both the spectral asymmetry formula (C1) and the symmetry relation $\mathcal{S}Q_W[A]\mathcal{S}^{-1} = (-1)^{d/2+2}Q_W[-A]$. This entails the following:

(1) The spectral asymmetry formula, expressed as $\frac{\Delta\phi_W}{2\pi} = \mathrm{ch}_W \int \mathfrak{C}$, implies that it is sufficient to focus on eigenvalues of Q_W (denoted by $q[A]$). These eigenvalues adhere to sign$q[A] =$ sign$\mathfrak{C}$, up to a possible A-field-independent sign.

(2) The symmetry relation $\mathcal{S}Q_W[A]\mathcal{S}^{-1} = (-1)^{d/2+2}Q_W[-A]$ dictates that for the eigenstate of Q_W (denoted by $|\psi[A]\rangle$) with eigenvalue $q[A]$, its symmetry-transformed counterpart (denoted by $\mathcal{S}^{-1}|\psi[-A]\rangle$) has eigenvalue $(-1)^{d/2+2}q[-A]$.

Consequently, we conclude that the eigenvalues of $|\psi[A]\rangle$ and $\mathcal{S}^{-1}|\psi[-A]\rangle$ share the same sign, i.e.,

$$\mathrm{sign}\{q[A] \times (-1)^{d/2+2}q[-A]\} = (-1)^{d+2} > 0, \tag{C14}$$

and thereby confirm the existence of symmetric pairs of $Q_W^{(+)}$ and of $Q_W^{(-)}$. We reemphasize that the symmetric pairs of sign$G$ have the opposite sign, and the symmetric pairs of $Q_W^{(\pm)}$ have the same sign.

b. An example for the symmetric pairs of sign(G) and Q_W

Here, we shall illustrate symmetric pairs discussed above in a concrete example, from which we reveal an emergent particle-hole symmetry, and dimensional reduction to zero-dimensional class-D insulators.

We consider the two-dimensional time-reversal symmetric Dirac model in Appendix B, and derive the Hamiltonian consisting of one symmetric pair of sign(G),

$$G = G_0 + m\sigma^z \otimes (\boldsymbol{n}\cdot\boldsymbol{\tau}),\ \boldsymbol{n} = (0,\ 0,\ 1) \tag{C15}$$

with

$$G_0 \equiv [i\partial_x - A_x(\boldsymbol{x})]\sigma^x \otimes \tau^0 + [i\partial_y - A_y(\boldsymbol{x})]\sigma^y \otimes \tau^0 \tag{C16}$$

and

$$\mathcal{T} = \mathcal{K}\sigma^y \otimes \tau^x, \tag{C17}$$

where the choice of $\boldsymbol{n}$ is made for simplicity. In Appendix B, we have demonstrated that under magnetic fields, the spectral asymmetry is from zero modes of G_0, in particular the difference in chiral zero modes (i.e., chiral matrix $\sigma^z \otimes \tau^0$). Hence, it is sufficient to focus on this zero-mode sector of G_0 (i.e., by setting G_0 to zero), rendering an effective Hamiltonian in the symmetric pair basis (with degeneracy $|\int \mathfrak{C}|$),

$$G_{(s)}[A] = m \times \mathrm{sign}(\mathfrak{C})\tau^z, \tag{C18}$$

with

$$\mathcal{S}_{(s)}G_{(s)}[A]\mathcal{S}_{(s)}^{-1} = -G_{(s)}[A] \text{ and } \mathcal{S}_{(s)} = \mathcal{K}\tau^x, \tag{C19}$$

where the "chiral matrix" σ^z drops out by restricting to one chiral sector because we are only interested in the difference of chiral modes. Clearly, this effective model possesses one symmetric pair of sign(G), signaled by the emergent "particle-hole symmetry" $\mathcal{S}_{(s)} = \mathcal{K}\tau^x$ $(\mathcal{S}_{(s)}^2 = 1)$. The latter is inherited from its parent $\mathcal{T}$ symmetry, such that σ^y drops out: The effect of σ^y (upon G) is to reverse both the sign of magnetic fields and mass, and thus acts trivially on $G_{(s)}$. Physically speaking, this is because magnetic field significantly constrains the "spin" degree of freedom, such that the operation upon spin (i.e., σ^y in $\mathcal{T}$) is irrelevant for the effective model. Finally, we remark that the magnetic field renders a dimensional reduction from two-dimensional time-reversal massive Dirac fermions (i.e., AII insulator) to zero-dimensional particle-hole massive ones (i.e., D insulator).

Built upon this, we can further construct the ensuing asymmetry matrix Q_W, containing one symmetric pair. This is based on the observation that in the basis of symmetric pairs, the only $\mathcal{W}$ allowed by symmetry is

$$\mathcal{W}_{(s)} = \tau^z, \text{ with } \mathcal{S}_{(s)}\mathcal{W}_{(s)}\mathcal{S}_{(s)}^{-1} = -\mathcal{W}_{(s)}, \tag{C20}$$

from which one can infer the effective Q_W, i.e.,

$$Q_{W,\ (s)} = \mathrm{sign}(m\mathfrak{C})\tau^0, \tag{C21}$$

consistent with our discussion in Appendix C 2, with $\xi = m \times \mathrm{sign}(\mathfrak{C})$.

APPENDIX D: RESULTS IN ODD SPATIAL DIMENSION FROM DIMENSIONAL REDUCTION

Here, we generalize our even-dimensional results to odd spatial dimensions, via the standard method of dimensional reduction [15,37,63]. This is achieved in two steps: (i) formulating the even-dimensional effective action for ϕ_W in terms of external fields, and (ii) deriving the ensuing odd-spatial-dimensional one, by integrating out one spatial dimension. From this odd dimensional ϕ_W, we can infer the ensuing order parameter, which falls into two categories, $\mathbb{Z}_2$ or $\mathbb{Z}$ $(2\mathbb{Z})$, determined by chiral symmetry.

We now implement this protocol, so as to derive ϕ_W in odd spatial dimensions. To this end, we start from an effective action for ϕ_W in $d = 2n$ spatial manifold $\mathcal{M}^{(2n)} = \mathcal{M}^{(2n-1)} \times S^1$, i.e.,

$$\phi_W \equiv \mathrm{ch}_W \times \int_{\mathcal{M}^{(2n)}} d^{2n}\boldsymbol{x}\, \mathcal{I}_W[w(\boldsymbol{x})] \times \mathfrak{C}^{(2n)}, \tag{D1}$$

where the superscript $(2n)$ emphasizes even spatial dimensions. $\mathfrak{C}^{(2n)}$ is the density of the homotopic invariant associated with background fields, so it is locally a total derivative $\mathfrak{C}^{(2n)} \equiv \partial_i \mathcal{K}_W^i$. We then perform an integration by part so as to facilitate the implementation of dimensional

reduction, i.e.,

$$\phi_W \equiv -\mathrm{ch}_W \int_{\mathcal{M}^{(2n-1)}} d^{2n-1}\boldsymbol{x}\, \partial_i \mathcal{I}_W[w(\boldsymbol{x})] \left(\oint_{S^1} d\boldsymbol{x}_{2n} \mathcal{K}_W^i \right), \tag{D2}$$

where we have assumed that $\mathcal{I}_W[w(\boldsymbol{x})]$ is independent of the $(2n)$th spatial dimension, and thus the superscript $i \neq 2n$. Then, we assume that $\mathcal{K}_W^i$ is of the Chern-Simons form, i.e., $\mathcal{K}_W^i = \frac{1}{n!}\frac{1}{(2\pi)^n}\epsilon^{ii_1i_2i_3\cdots}A_{i_1}\partial_{i_2}A_{i_3}\ldots$, where A_i can be the electromagnetic gauge field, or the gauge field from skyrmions [60]. After these preparations, we shall derive the odd-dimensional action by integrating out one spatial dimension, implemented by the following:

(i) taking the dependence on the extra $2n$th spatial coordinate dependence exclusively via A_{2n};

(ii) inserting half a flux quantum along $\boldsymbol{x}_{2n}$, i.e., $\oint A_{2n} d\boldsymbol{x}_{2n} = -\pi$.

Together, we find the following ϕ_W for the odd-spatial-dimension descendant,

$$\frac{\phi_W}{\pi} = \mathrm{ch}_W \int_{\mathcal{M}^{(2n-1)}} \partial_i \mathcal{I}_W[w(\boldsymbol{x})] \frac{1}{2\pi} \mathfrak{C}^{(2n-2)} \in \mathrm{ch}_W \times \mathbb{Z}, \tag{D3}$$

where $\mathfrak{C}^{(2n-2)}$ is independent of $\boldsymbol{x}_i$, and thus $\int d\boldsymbol{x}_i \partial_i \mathcal{I}_W \in 2\pi\mathbb{Z}$ due to spatial periodicity.

Built upon the formula (D3), we now discuss about the ensuing topological order parameter, enumerated below:

(1) For the nonchiral symmetric class, the mixed-state topological order parameter is taken to be $\frac{\phi_W}{\pi} = 0,\ 1 \bmod 2 \in \mathbb{Z}_2$, which renders a $\mathbb{Z}_2$ invariant. In particular, this $\mathbb{Z}_2$ accounts for the ambiguity encoded in the map between even-dimensional parent states and their odd-dimensional descendant.

(2) For the chiral symmetric class, the descendant state belongs to the $\mathbb{Z}$ ($2\mathbb{Z}$) class instead, as chiral symmetry resolves the map ambiguity [12], which can be detected by $\frac{\phi_W}{\pi} \in \mathbb{Z}$.

Example: Complex fermion in the one-dimensional DIII class

Based on the strategy outlined in the last part, now we construct a mixed-state topological order parameter in details, by properly choosing $w[\boldsymbol{x}]$. Following the dimensional reduction sketched in Fig. 1 in the main text, we shall focus on the second descendant, e.g., blue $\mathbb{Z}_2$ in Table I, while for other classes, one can obtain the mixed-state order parameter via the polarization operator (e.g., generalization of the ensemble geometric phase [35,37]).

To detect the underlying topology, we shall make a slight modification of the probe operator, according to

$$\frac{2\pi \boldsymbol{x}_\alpha}{N_i}\mathcal{W} \to \frac{2\pi \boldsymbol{x}_\alpha}{N_\alpha}\frac{1}{2}(\mathbb{I} + \mathcal{W}), \tag{D4}$$

where the subscript α refers to the α-spatial direction. $\frac{1}{2}(\mathbb{I} + \mathcal{W})$ is a projection operator, activating half the degree of freedom. This modification is necessary because $\mathrm{ch}_W \in 2\mathbb{Z}$ for the $\mathbb{Z}_2$ class (blue in Table I), inherited from the parent $2\mathbb{Z}$ class (brown in Table I). In turn, by taking $w = \frac{2\pi \boldsymbol{x}_\alpha}{N_\alpha}$, $\phi_W \in 2\pi\mathbb{Z}$, and thus $e^{i\phi_W} = +1$. To cure this and improve the resolution of $e^{i\phi_W}$, we utilize Eq. (D4) to activate half the degree of freedom. (For superconductors, this modification is not needed, i.e., $e^{i\phi_W} = \pm 1$ as explained in Appendix G.)

Physically speaking, this modification impacts on both the original probe operator (e.g., $\frac{\pi}{N_\alpha}\boldsymbol{x}_\alpha\mathcal{W}$) and the temporal component of the U(1) gauge field (e.g., $A_0 = \frac{\pi}{N_\alpha}\boldsymbol{x}_\alpha$, via the overall prefactor $\frac{1}{2}$). It is the modification of the probe operator which provides us with a signal distinguishing different (blue) $\mathbb{Z}_2$ mixed states, i.e., $e^{i\frac{1}{2}\phi_W} = \pm 1$, because w associated with $\mathcal{W}$ takes $\frac{1}{2}$ of its original value. The modification of the U(1) part preserves the spatial periodicity, i.e., $\boldsymbol{x}_\alpha \to \boldsymbol{x}_\alpha + N_\alpha$: Since the U(1) action for (blue) $\mathbb{Z}_2$ is known to be nontopological [37,51,84], so we expect its contribution to ϕ_W vanishes. Numerically, we confirm this in the DIII complex fermion class (see Fig. 3).

APPENDIX E: NUMERICAL RESULTS FOR NONEQUILIBRIUM MIXED STATE

We apply our mixed-state order parameter to study the nonequilibrium dynamics of mixed states, which arise from exposing the pure ground state of a Hamiltonian to dissipative processes. Concretely, we start from the ground state of the (modified) BHZ model (AII insulator), with Hamiltonian

$$H = \begin{pmatrix} H_0(\boldsymbol{k}) & -i\Delta\tau^y \\ i\Delta\tau^y & H_0^*(-\boldsymbol{k}) \end{pmatrix}, \quad \mathcal{T} = \sigma^y \otimes \tau^0 \mathcal{K}. \tag{E1}$$

$H_0 = \boldsymbol{d}\cdot\boldsymbol{\tau}$ with $\boldsymbol{d} = [\sin(k_x),\ \sin(k_y),\ m + \cos(k_x) + \cos(k_y))]$ is the Qi-Wu-Zhang model [85], and time-reversal symmetry is implemented by $\mathcal{T}$.

We subsequently examine the ground state subjected to Lindblad dynamics, characterized by linear Lindblad operators (with Hamiltonian switched off)

$$\hat{L}_i^{(l)} = \sqrt{\gamma_l}\frac{1 + \tau^z \otimes \sigma^0}{2}\hat{\psi}_i, \quad \hat{L}_i^{(g)} = \sqrt{\gamma_g}\frac{1 - \tau^z \otimes \sigma^0}{2}\hat{\psi}_i^\dagger, \tag{E2}$$

which preserves the time-reversal symmetry [48,86]. These processes by themselves target a trivial pure steady state, i.e., $|\psi_{\mathrm{target}}\rangle = \prod_i \hat{\psi}_{i,\ a=2}^\dagger \hat{\psi}_{i,\ a=4}^\dagger |0\rangle$, where $|0\rangle$ is for the vacuum without particle, and the subscript a for internal indices.

For the probe operator, possible choices for the $\mathcal{W}$ matrix are then $\mathcal{W} = \{\boldsymbol{\sigma} \otimes \tau^{x,\ z,\ 0},\ \sigma^0 \otimes \tau^y\}$. Numerical results are presented in Fig. 4, which include the plot of the Loschmidt echo $|\mathcal{Z}_W[w = \pi]|^2$ at $w = \pi$, or its rate function $\lambda(t) \equiv -\frac{\ln|\mathcal{Z}_W[w=\pi]|^2}{N_x \times N_y}$] in the left panel, and mixed-state order parameter in the right panel. Here, both the rate function $\lambda(t)$ and $\frac{\Delta\phi_W}{2\pi}$ provide a sharp signature distinguishing different phases.

APPENDIX F: PHASE SIGNAL ϕ_W IN COLD-ATOMIC ENSEMBLES

In the main text, we have discussed numerical results for ϕ_W within the canonical ensemble, i.e., for a fixed number of particles. Here we demonstrate the effectiveness of the order parameter $\frac{\Delta\phi_W}{2\pi}$ in full counting statistic measurements with cold atoms. These measurements will be carried out by repeating the counting experiment many times, with two key characteristics: (1) Within each run, the particle number is fixed, and (2) for every run, however, the particle number

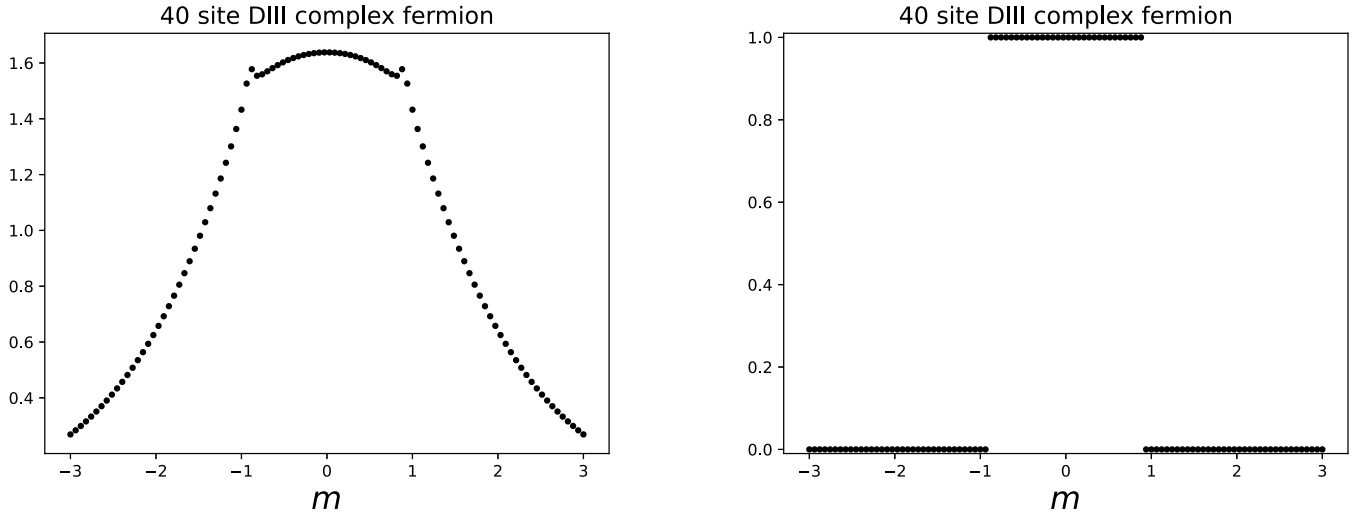

FIG. 3. Numerical results for the 1D DIII complex fermions, with $G = -(\sin k_x \sigma^z) \otimes \tau^x + (m + \cos k_x)\sigma^0 \otimes \tau^z$, and k_x for momentum. Here, $\mathcal{W} = \boldsymbol{n} \cdot \boldsymbol{\sigma} \otimes \tau^0$ is the spin matrix, with $\boldsymbol{n}$ a randomly sampled unit vector. Left panel: plot of $-2 \ln |\mathrm{Tr}(\hat{\rho}\hat{U})|/N_x$ as a function of m, with site number N_x. Here, we take $\hat{U} = (-1)^{N_x+1} e^{-i \sum_i \hat{\Psi}_i^\dagger \frac{2\pi x}{N_x} \frac{1}{2}(\mathbb{I}+\mathcal{W})\hat{\Psi}_i}$, and $(-1)^{N_x+1}$ is the factor in reference to the topological trivial phase. This clearly exhibits cusp around the topological transition point (e.g., $m = \pm 1$). Right panel: plot of (modified) ϕ_W as a function of m, showing a sharp transition between different topological phases.

might be different, governed by some probability distribution function for the particle number. In Fig. 5, we present numerical results incorporating these specifics for the modified BHZ model [Eq. (10) in the main text], adopting a Poisson distribution function to model the mean particle number at half-filling for definiteness [see Fig. 5(a)]. The results depicted in Fig. 5(b) clearly demonstrate that $\frac{\Delta\phi_W}{2\pi}$ efficiently differentiates between topological and trivial phases.

APPENDIX G: RESULTS FOR SUPERCONDUCTORS (MAJORANA FERMIONS)

We present results for superconductors (Majorana fermions), which includes (i) the relation between spectral asymmetry and fermion parity, and (ii) the construction of a mixed-state topological order parameter.

We first introduce the necessary notation. In the context of superconductors, the U(1) symmetry is broken down to the discrete $\mathbb{Z}_2$ fermion parity symmetry. Accordingly, we work in the Nambu basis, and the modular Hamiltonian is expressed as

$$\hat{G} = \hat{\Psi}^\dagger G \hat{\Psi}, \quad \text{with } \hat{\Psi} \equiv (\hat{\psi},\ \hat{\psi}^\dagger)^T, \tag{G1}$$

where the first quantized operator G embodies particle-hole symmetry.

1. Fermion parity and spectral asymmetry for Majorana

We demonstrate that fermion parity detects spectral properties of the modular Hamiltonian G. Namely, due to particle-hole symmetry, the eigenvalues of the matrix G appear in pairs with opposite sign, i.e., $\{\lambda_n,\ -\lambda_n\}$, where λ_n

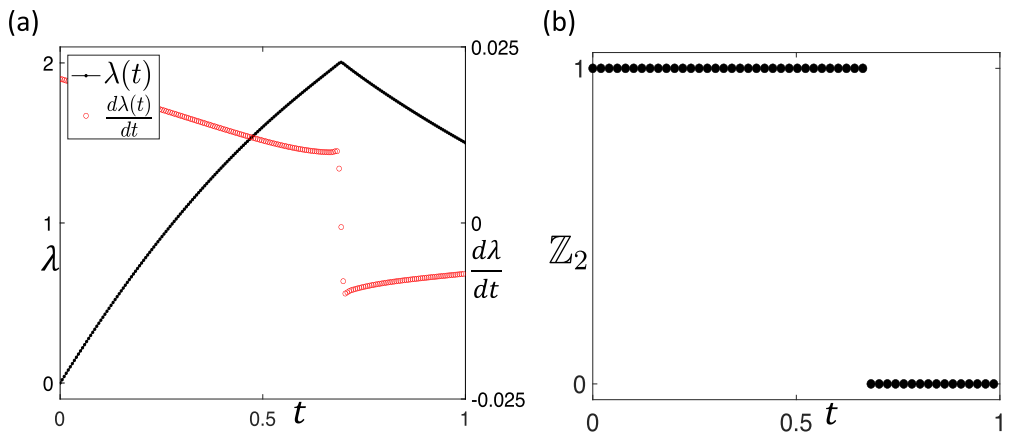

FIG. 4. Numerical results for mixed-state open system evolution starting from a ground state (with one magnetic flux quantum inserted, site number 15×15, $m = 1$, $\Delta = 0.5$). The left panel shows the amplitude of the Loschmidt echo at $w = \pi$, i.e., $\lambda(t) \equiv -\frac{\ln |\mathcal{Z}_W[w=\pi]|^2}{N_x \times N_y}$, which exhibits a cusp around the transition point. The right panel presents $\frac{1}{2}\frac{\Delta\phi_W}{2\pi}$ as a function of t, with gapped Q_W.

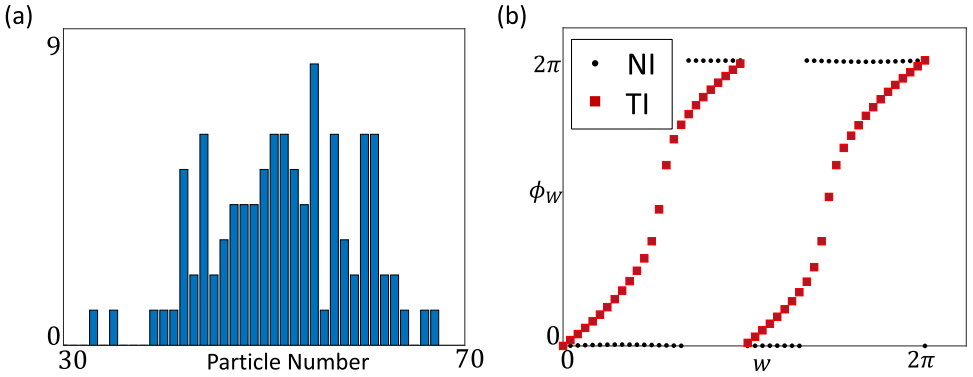

FIG. 5. Numerical results for the phase signal ϕ_W in cold-atomic ensembles, focusing on the modified BHZ model on a 5×5 lattice; each lattice site hosts four states. The ensemble-averaged particle number corresponding to half-filling is 50, and we set the model parameters to $\beta = 3$ and $\Delta = 0.5$. In (a), we have sampled 50 runs from the Poisson distribution, where the y axis represents the frequency of particle number. In (b), we delineate the ensemble-averaged phase signal for both topological insulators (TI), and normal insulators (NI), exemplified by $m = 1, 3$, respectively. The ensemble-averaged phase signal for N_s samples is defined as $\phi_W \equiv \arg[\frac{1}{N_s}\sum_{n=1}^{N_s} \mathcal{Z}_W^{(n)}]$, with n the sample index.

can be positive or negative. We then divide these particle-hole pairs to two different classes, e.g., $\{\lambda_1,\ \lambda_2,\ \dots\}$ and $\{-\lambda_1,\ -\lambda_2,\ \dots\}$, such that $G = \oplus_n \begin{pmatrix} 0 & i\lambda_n \\ -i\lambda_n & 0 \end{pmatrix}$. It turns out that the fermion parity $(-1)^{\hat{Q}}$ crucially hinges on the spectral asymmetry of $\{\lambda_1,\ \lambda_2,\ \dots\}$,

$$\mathrm{Im}\ln \mathrm{Tr}[(-1)^{\hat{Q}}\hat{\rho}] = -\frac{\pi}{2}N + \frac{\pi}{2}\sum_n \mathrm{sign}(\lambda_n), \tag{G2}$$

where N is for the total particle number, and we have used the following identity (see, for example, [79,87]):

$$\mathrm{Tr}(\hat{\rho}e^{-i\pi\hat{Q}}) = (-i)^N \mathrm{Pf}(\tanh G). \tag{G3}$$

This indicates that the fermion parity probes the asymmetry of λ_n.

2. Probe operator for superconductors in the prime series

We now turn to Majorana models in the prime series, which includes examples like the Kitaev chain, and the two-dimensional (2D) p-wave chiral superconductor. The superconductor no longer enjoys U(1) symmetry, but still we can induce a spectral asymmetry via a $\mathbb{Z}_2$ gauge field, implemented via antiperiodic spatial boundary conditions, based upon which we construct a mixed-state order parameter.

The probe operator, similar to the complex fermion counterpart, is taken to be

$$e^{-iw\hat{Q}}, \quad \hat{Q} = \sum_{i,\ a} \hat{\psi}^{\dagger}_{i,\ a}\psi_{i,a}. \tag{G4}$$

For the mixed-state density matrix, we need to replace the U(1) gauge fields by an alternative construction. In fact, $\mathbb{Z}_2$ gauge fields can be utilized to activate topological charge. This can be implemented in the density matrix by twisted boundary conditions according to

$$\hat{\rho} = e^{-\hat{G}}|_{(s_1,s_2,\dots)}, \tag{G5}$$

where $s_1, s_2 \cdots = 0,\ \pi$ for the periodic and antiperiodic boundary condition along ith spatial direction. The ensuing mixed-state order parameter is then defined as the winding number of the following phase:

$$\phi_W(w) \equiv \arg\left[\prod_{s_1,s_2,\cdots=0,\pi} \mathrm{Tr}(\hat{\rho}e^{-iw\hat{Q}})^{\nu_{\{s\}}}\right], \tag{G6}$$

where $\nu_{\{s\}} = +1\ (-1)$ for $\{s\} = (s_1, s_2, \dots)$ containing even (odd) number of 0. Here, the product provides a normalization which ensures that the winding number $\phi_W(w)$ is only from insertion of $\mathbb{Z}_2$ gauge field in all spatial directions. For example, the factor $-\frac{\pi}{2}N$ in Eq. (G2) is canceled, which shall be further illustrated below, via examples.

We are now in the position to construct the associated effective action, from which we can infer the descendant $\mathbb{Z}_2$ invariant, via the method of dimensional reduction. That is, the action is

$$\phi_W(w) = \mathrm{ch}_W \int \mathcal{I}_W[w]\frac{a_1}{\pi} \times \frac{a_2}{\pi}\dots, \tag{G7}$$

with

$$\mathrm{ch}_W \in \mathbb{Z},\ \mathcal{I}_W[w]|_{w=0}^{w=2\pi} = 2\pi,\ \text{and}\ \mathcal{I}_W[w=\pi] = \pi, \tag{G8}$$

where a_i is the $\mathbb{Z}_2$ gauge field for the ith direction, such that $\oint a_i = s_i$. We have assumed that $\mathcal{I}_W[w]$ is a smooth function of w for a gapped system. Also, $\mathcal{I}_W[w=\pi] = \pi$ is from Hermiticity, i.e., $\phi_W(w) = -\phi_W(-w)$. Taking one spatial dimension as an example, this reproduces the result in Ref. [66], by taking $\mathcal{I}_W[w] = w$. Finally, it is worth mentioning that the effective action shares the same form in all dimensions, as the dimensional reduction is implemented by integrating out a π flux inserted along the extra dimension.

As an illustration, we consider the $w = \pi$ point, which determines the evenness or oddness of the winding number (i.e., ch_W). In the one-dimensional case, we find

$$e^{i\phi_W(\pi)} = \mathrm{sign}\left[\frac{\langle(-1)^{\hat{Q}}\rangle|_{s_1=\pi}}{\langle(-1)^{\hat{Q}}\rangle|_{s_1=0}}\right], \tag{G9}$$

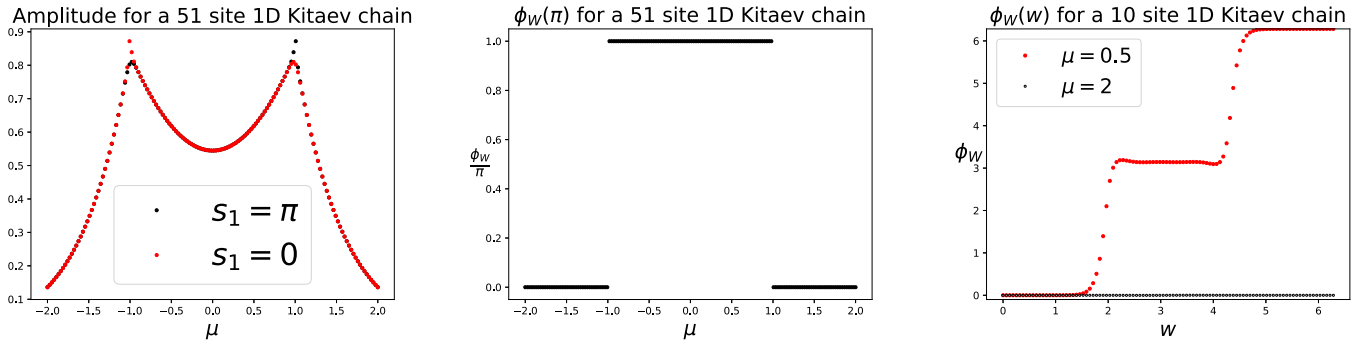

FIG. 6. Numerical results for the 1D Kitaev chain. Left panel: plot of $-2\ln|\mathrm{Tr}[\hat{\rho}(-1)^{\hat{Q}}]|_{s_1=0,\pi}|/N_x$ as a function of μ, which exhibits singular points around the topological transition point ($\mu = \pm 1$). Middle panel: plot of $\frac{\phi_W(w=\pi)}{\pi}$ as a function of μ, which reconstructs the zero-temperature phase diagram. Right panel: plot of $\phi_W(w)$ at $\mu = 0.5, 2$ as a function of w, which shows that ϕ_W possesses different winding numbers in the topologically trivial and nontrivial phases.

which reproduces the $\mathbb{Z}_2$ index for Majorana fermions [66,88]. We see the role of the denominator, canceling out irrelevant factors, e.g., $(-i)^N$ in Eq. (G3). Meanwhile, the two-dimensional counterpart is

$$e^{i\phi_W(\pi)} = \mathrm{sign}\left[\frac{\langle(-1)^{\hat{Q}}\rangle|_{s_1=\pi,s_2=\pi}\langle(-1)^{\hat{Q}}\rangle|_{s_1=0,s_2=0}}{\langle(-1)^{\hat{Q}}\rangle|_{s_1=0,s_2=\pi}\langle(-1)^{\hat{Q}}\rangle|_{s_1=\pi,s_2=0}}\right], \tag{G10}$$

which is reminiscent of the invariant defined in Ref. [89]. Physically, this describes the pumping of the one-dimensional fermion parity [e.g., Eq. (G9)], after insertion of a π flux (i.e., $s_2 = \pi$).

Numerical results for ϕ_W in one and two dimensions

To further support our results above, we shall present numerical results in the Kitaev chain, and the two-dimensional chiral p-wave superconductors.

For the Kitaev chain, the modular Hamiltonian is

$$\hat{G} = -\mu\sum_i(\hat{\psi}_i^\dagger\hat{\psi}_i + \mathrm{H.c.}) - t\sum_i(\hat{\psi}_{i+1}^\dagger\hat{\psi}_i + \mathrm{H.c.}) + \Delta\sum_i(\hat{\psi}_{i+1}\hat{\psi}_i + \mathrm{H.c.}). \tag{G11}$$

For later convenience, we shall set $t = \Delta = 1$, so this model is topologically nontrivial (trivial) for $|\mu| < 1$ ($|\mu| > 1$). Meanwhile, the twisted spatial boundary condition is implemented via

$$-te^{is_1}\hat{\psi}_1^\dagger\hat{\psi}_{N_x} \text{ and } \Delta e^{is_1}\hat{\psi}_1\hat{\psi}_{N_x}, \text{ with } s_1 = 0,\ \pi. \tag{G12}$$

Numerical results for the Kitaev chain are presented in Fig. 6. The left panel and the middle panel demonstrate that $\frac{\phi_W(w=\pi)}{\pi}$ successfully captures the topology in different phase, and the transition point manifests itself as a cusp in the amplitude, $\lambda \equiv -\frac{\ln|\mathcal{Z}_W|^2}{N_x}$. The right panel displays ϕ_W as a function of w, which does exhibit different winding for the topologically trivial and nontrivial phases. Note that the trace formula for the product of two Majorana Gaussian operators is not known

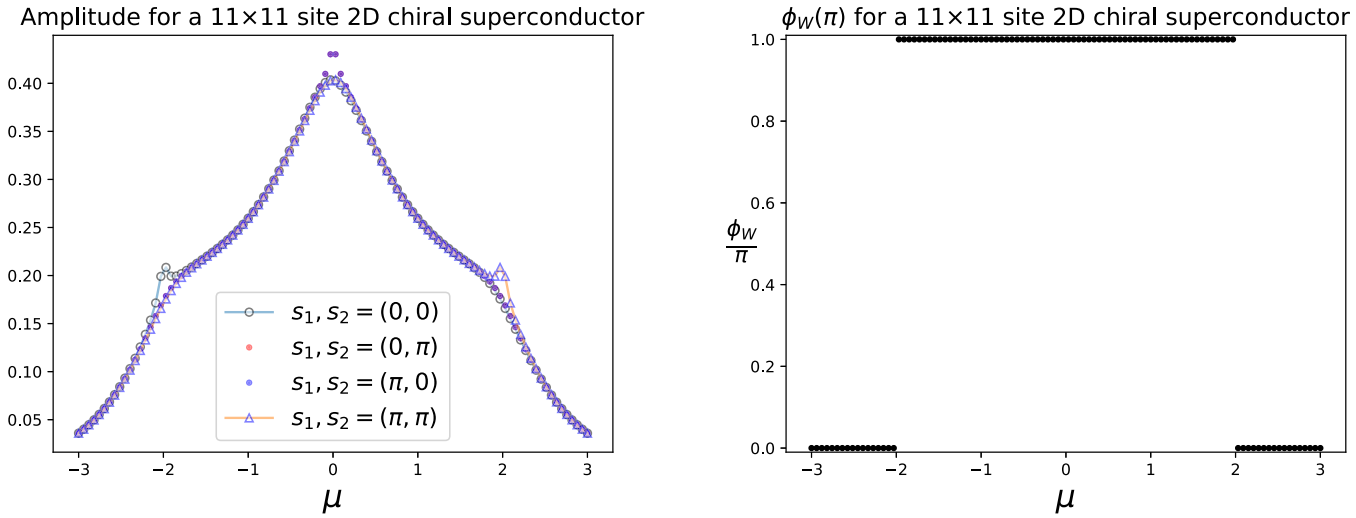

FIG. 7. Numerical results for the 2D chiral superconductor. Left panel: plot of $-2\ln|\mathrm{Tr}[\hat{\rho}(-1)^{\hat{Q}}]|_{s_1,s_2=0,\pi}|/(N_x \times N_y)$ as a function of μ, which exhibits a singular point around the topological phase transition point ($\mu = \pm 2$). Right panel: plot of $\frac{\phi_W(w=\pi)}{\pi}$ as a function of μ, which shows that $\frac{\phi_W(w=\pi)}{\pi}$ detects the topologically trivial and nontrivial phases.

except when one of the operators is the fermion parity (to the best of our knowledge) [79], so here we used the method of exact diagonalization.

For the two-dimensional chiral p-wave superconductor, the modular Hamiltonian is

$$\begin{aligned}\hat{G} = &\sum_{m,n}[-t(\hat{\psi}^{\dagger}_{m+1,n}\hat{\psi}_{m,n} + \text{H.c.}) - t(\hat{\psi}^{\dagger}_{m,n+1}\hat{\psi}_{m,n} + \text{H.c.})] \\ &- \sum_{m,n}\mu(\hat{\psi}^{\dagger}_{m,n}\hat{\psi}_{m,n} + \text{H.c.}) \\ &+ \sum_{m,n}[(\Delta\hat{\psi}^{\dagger}_{m+1,n}\hat{\psi}^{\dagger}_{m,n} + \text{H.c.}) \\ &+ (i\Delta\hat{\psi}^{\dagger}_{m,n+1}\hat{\psi}^{\dagger}_{m,n} + \text{H.c.})], \end{aligned} \tag{G13}$$

and the twisted boundary condition is implemented similar to the Kitaev chain. Also, for later convenience, we set $\Delta = t = 1$, and this model is topologically nontrivial (trivial) for $|\mu| < 2$ ($|\mu| > 2$). Numerical results are presented in Fig. 7, which confirms that $\frac{\phi_W(w=\pi)}{\pi}$ probes the underlying topology for mixed states.

3. Probe operator for superconductors in the $\mathbb{Z}_2$ class

For superconductors in the $\mathbb{Z}_2$ class, parallel to their complex fermion counterparts, we are required to choose $\mathcal{W}$ differently from $\mathbb{I}$ in order to resolve the topological signal. In turn, constraints for $\mathcal{W}$ are similar, except for the following:

(1) $\mathcal{W}$ should be antisymmetric, due to the anticommuting nature of Majorana.

(2) The $\mathcal{W} \to \frac{1}{2}\mathcal{W}$ with a $\frac{1}{2}$ factor, from the redundancy in the Nambu space.

This construction hinges on the following identity for Majorana fermions:

$$[\text{Tr}(e^{-\hat{\gamma}A\hat{\gamma}}e^{-\hat{\gamma}B\hat{\gamma}})]^2 = \det(\mathbb{I} + e^{-2A}e^{-2B}), \tag{G14}$$

where the anticommutation relation of $\hat{\gamma}$ is $\{\hat{\gamma}_a,\ \hat{\gamma}_b\} = \delta_{ab}$. A, B are skew symmetric, from the anticommutation relations, reproducing 1. The Majorana Gaussian operator $e^{-\hat{\gamma}A\hat{\gamma}}$ appears on the right-hand side as $e^{-\mathbf{2}A}$, leading to 2.

[1] I. Bloch, J. Dalibard, and S. Nascimbène, Quantum simulations with ultracold quantum gases, Nat. Phys. **8**, 267 (2012).

[2] J. I. Cirac and P. Zoller, Goals and opportunities in quantum simulation, Nat. Phys. **8**, 264 (2012).

[3] N. Goldman, J. C. Budich, and P. Zoller, Topological quantum matter with ultracold gases in optical lattices, Nat. Phys. **12**, 639 (2016).

[4] E. Altman, K. R. Brown, G. Carleo, L. D. Carr, E. Demler, C. Chin, B. DeMarco, S. E. Economou, M. A. Eriksson, K.-M. C. Fu, M. Greiner, K. R. Hazzard, R. G. Hulet, A. J. Kollár, B. L. Lev, M. D. Lukin, R. Ma, X. Mi, S. Misra, C. Monroe *et al.*, Quantum simulators: Architectures and opportunities, PRX Quantum **2**, 017003 (2021).

[5] J. C. Halimeh, M. Aidelsburger, F. Grusdt, P. Hauke, and B. Yang, Cold-atom quantum simulators of gauge theories, Nat. Phys. **21**, 25 (2025).

[6] G. Semeghini, H. Levine, A. Keesling, S. Ebadi, T. T. Wang, D. Bluvstein, R. Verresen, H. Pichler, M. Kalinowski, R. Samajdar, A. Omran, S. Sachdev, A. Vishwanath, M. Greiner, V. Vuletić, and M. D. Lukin, Probing topological spin liquids on a programmable quantum simulator, Science **374**, 1242 (2021).

[7] K. J. Satzinger, Y.-J. Liu, A. Smith, C. Knapp, M. Newman, C. Jones, Z. Chen, C. Quintana, X. Mi, A. Dunsworth, C. Gidney, I. Aleiner, F. Arute, K. Arya, J. Atalaya, Babbush *et al.*, Realizing topologically ordered states on a quantum processor, Science **374**, 1237 (2021).

[8] J. Preskill, Quantum Computing in the NISQ era and beyond, Quantum **2**, 79 (2018).

[9] X. Mi, A. Michailidis, S. Shabani, K. Miao, P. Klimov, J. Lloyd, E. Rosenberg, R. Acharya, I. Aleiner, T. Andersen *et al.*, Stable quantum-correlated many body states via engineered dissipation, Science **383**, 1332 (2024).

[10] A. Altland and M. R. Zirnbauer, Nonstandard symmetry classes in mesoscopic normal-superconducting hybrid structures, Phys. Rev. B **55**, 1142 (1997).

[11] C. Nayak, S. H. Simon, A. Stern, M. Freedman, and S. Das Sarma, Non-Abelian anyons and topological quantum computation, Rev. Mod. Phys. **80**, 1083 (2008).

[12] S. Ryu, A. P. Schnyder, A. Furusaki, and A. W. W. Ludwig, Topological insulators and superconductors: Tenfold way and dimensional hierarchy, New J. Phys. **12**, 065010 (2010).

[13] A. Kitaev, Fault-tolerant quantum computation by anyons, Ann. Phys. **303**, 2 (2003).

[14] A. Kitaev, Periodic table for topological insulators and superconductors, AIP Conf. Proc. **1134**, 22 (2009).

[15] X.-L. Qi and S.-C. Zhang, Topological insulators and superconductors, Rev. Mod. Phys. **83**, 1057 (2011).

[16] M. Z. Hasan and C. L. Kane, *Colloquium:* Topological insulators, Rev. Mod. Phys. **82**, 3045 (2010).

[17] X. Chen, Z.-C. Gu, Z.-X. Liu, and X.-G. Wen, Symmetry protected topological orders and the group cohomology of their symmetry group, Phys. Rev. B **87**, 155114 (2013).

[18] A. W. W. Ludwig, Topological phases: Classification of topological insulators and superconductors of non-interacting fermions, and beyond, Phys. Scr. **2016**, 014001 (2015).

[19] C.-K. Chiu, J. C. Y. Teo, A. P. Schnyder, and S. Ryu, Classification of topological quantum matter with symmetries, Rev. Mod. Phys. **88**, 035005 (2016).

[20] S. Diehl, A. Micheli, A. Kantian, B. Kraus, H. P. Büchler, and P. Zoller, Quantum states and phases in driven open quantum systems with cold atoms, Nat. Phys. **4**, 878 (2008).

[21] S. Diehl, E. Rico, M. A. Baranov, and P. Zoller, Topology by dissipation in atomic quantum wires, Nat. Phys. **7**, 971 (2011).

[22] L. M. Sieberer, M. Buchhold, J. Marino, and S. Diehl, Universality in driven open quantum matter, Rev. Mod. Phys. **97**, 025004 (2025).

[23] X. Cao, A. Tilloy, and A. D. Luca, Entanglement in a fermion chain under continuous monitoring, SciPost Phys. **7**, 024 (2019).

[24] O. Alberton, M. Buchhold, and S. Diehl, Entanglement transition in a monitored free-fermion chain: From extended criticality to area law, Phys. Rev. Lett. **126**, 170602 (2021).
[25] M. P. Fisher, V. Khemani, A. Nahum, and S. Vijay, Random quantum circuits, Annu. Rev. Condens. Matter Phys. **14**, 335 (2023).
[26] I. Poboiko, I. V. Gornyi, and A. D. Mirlin, Measurement-induced phase transition for free fermions above one dimension, Phys. Rev. Lett. **132**, 110403 (2024).
[27] A. Kitaev, Anyons in an exactly solved model and beyond, Ann. Phys. **321**, 2 (2006).
[28] S. Bravyi, M. Englbrecht, R. König, and N. Peard, Correcting coherent errors with surface codes, npj Quantum Inf. **4**, 55 (2018).
[29] F. Venn, J. Behrends, and B. Béri, Coherent-error threshold for surface codes from Majorana delocalization, Phys. Rev. Lett. **131**, 060603 (2023).
[30] Z.-M. Huang, L. Colmenarez, M. Müller, and S. Diehl, Coherent information as a mixed-state topological order parameter of fermions, arXiv:2412.12279.
[31] O. Viyuela, A. Rivas, and M. A. Martin-Delgado, Uhlmann phase as a topological measure for one-dimensional fermion systems, Phys. Rev. Lett. **112**, 130401 (2014).
[32] O. Viyuela, A. Rivas, and M. A. Martin-Delgado, Two-dimensional density-matrix topological fermionic phases: Topological Uhlmann numbers, Phys. Rev. Lett. **113**, 076408 (2014).
[33] Z. Huang and D. P. Arovas, Topological indices for open and thermal systems via Uhlmann's phase, Phys. Rev. Lett. **113**, 076407 (2014).
[34] J. C. Budich and S. Diehl, Topology of density matrices, Phys. Rev. B **91**, 165140 (2015).
[35] C.-E. Bardyn, L. Wawer, A. Altland, M. Fleischhauer, and S. Diehl, Probing the topology of density matrices, Phys. Rev. X **8**, 011035 (2018).
[36] L. Wawer and M. Fleischhauer, $\mathbb{Z}_2$ topological invariants for mixed states of fermions in time-reversal invariant band structures, Phys. Rev. B **104**, 214107 (2021).
[37] Z.-M. Huang, X.-Q. Sun, and S. Diehl, Topological gauge theory for mixed Dirac stationary states in all dimensions, Phys. Rev. B **106**, 245204 (2022).
[38] E. Sjöqvist, A. K. Pati, A. Ekert, J. S. Anandan, M. Ericsson, D. K. L. Oi, and V. Vedral, Geometric phases for mixed states in interferometry, Phys. Rev. Lett. **85**, 2845 (2000).
[39] L. S. Levitov and G. B. Lesovik, Charge distribution in quantum shot noise, Pisma Zh. Eksp. Teor. Fiz. **58**, 225 (1993) [JETP Lett. **58**, 230 (1993)].
[40] W. S. Bakr, J. I. Gillen, A. Peng, S. Fölling, and M. Greiner, A quantum gas microscope for detecting single atoms in a Hubbard-regime optical lattice, Nature (London) **462**, 74 (2009).
[41] J. F. Sherson, C. Weitenberg, M. Endres, M. Cheneau, I. Bloch, and S. Kuhr, Single-atom-resolved fluorescence imaging of an atomic Mott insulator, Nature (London) **467**, 68 (2010).
[42] E. Haller, J. Hudson, A. Kelly, D. A. Cotta, B. Peaudecerf, G. D. Bruce, and S. Kuhr, Single-atom imaging of fermions in a quantum-gas microscope, Nat. Phys. **11**, 738 (2015).
[43] A. Mazurenko, C. S. Chiu, G. Ji, M. F. Parsons, M. Kanász-Nagy, R. Schmidt, F. Grusdt, E. Demler, D. Greif, and M. Greiner, A cold-atom Fermi–Hubbard antiferromagnet, Nature (London) **545**, 462 (2017).
[44] S. Humeniuk and H. P. Büchler, Full counting statistics for interacting fermions with determinantal quantum Monte Carlo simulations, Phys. Rev. Lett. **119**, 236401 (2017).
[45] M. Aidelsburger, S. Nascimbene, and N. Goldman, Artificial gauge fields in materials and engineered systems, C. R. Phys. **19**, 394 (2018).
[46] R. Citro and M. Aidelsburger, Thouless pumping and topology, Nat. Rev. Phys. **5**, 87 (2023).
[47] C.-E. Bardyn, M. A. Baranov, C. V. Kraus, E. Rico, A. İmamoğlu, P. Zoller, and S. Diehl, Topology by dissipation, New J. Phys. **15**, 085001 (2013).
[48] A. Altland, M. Fleischhauer, and S. Diehl, Symmetry classes of open fermionic quantum matter, Phys. Rev. X **11**, 021037 (2021).
[49] For example, w can be $\frac{2\pi x_\alpha}{N_\alpha}$ with $\boldsymbol{x}_\alpha$ the coordinate and N_α the site number along the αth spatial dimension.
[50] The wording "particle-hole symmetry" is standard but abusive; see [10] for the construction of a true particle-hole symmetry.
[51] X.-L. Qi, T. L. Hughes, and S.-C. Zhang, Chiral topological superconductor from the quantum Hall state, Phys. Rev. B **82**, 184516 (2010).
[52] Complex fermions in odd spatial dimension belonging to the second descendant states require the following modification: $\mathcal{W} \to \frac{1}{2}(\mathbb{I} + \mathcal{W})$, which singles out the eigenvectors with positive eigenvalues. This stems from $e^{i\phi_\mathcal{W}} = +1$ for $\mathcal{W}$, reflecting an even Chern number for its parent state. Instead, ultilizing $\frac{1}{2}(\mathbb{I} + \mathcal{W})$ results in $e^{i\phi_\mathcal{W}} = \pm 1$, revealing the underlying topology (for details, see Appendix D. For superconductors in the same class, such modification is not needed since they contain only half the degree of freedom compared to their complex fermion counterpart.
[53] O. Knill, On Atiyah-Singer and Atiyah-Bott for finite abstract simplicial complexes, arXiv:1708.06070.
[54] M. F. Atiyah, V. K. Patodi, and I. M. Singer, Spectral asymmetry and Riemannian geometry. I, in *Mathematical Proceedings of the Cambridge Philosophical Society*, Vol. 77 (Cambridge University Press, Cambridge, 1975), pp. 43–69.
[55] M. F. Atiyah, V. K. Patodi, and I. M. Singer, Spectral asymmetry and Riemannian geometry. III, in *Mathematical Proceedings of the Cambridge Philosophical Society*, Vol. 79 (Cambridge University Press, Cambridge, 1976), pp. 71–99.
[56] We have neglected a term $\mathrm{tr}\mathcal{W}$. This is because 1. for $\mathcal{W} = \mathbb{I}$, it gives a state-independent phase factor; 2. in the presence of time-reversal or particle-hole symmetry, it vanishes. Let us make this explicit for time-reversal symmetry: 1 and 2 imply that $\mathrm{Tr}\mathcal{W} = -\mathrm{Tr}\mathcal{W} = 0$.
[57] G. E. Volovik, *The Universe in a Helium Droplet* (Oxford University Press, Oxford, 2003).
[58] Z.-M. Huang and S. Diehl, Interaction-induced topological phase transition at finite temperature, Phys. Rev. Lett. **134**, 053002 (2025).
[59] A. J. Niemi and G. W. Semenoff, Spectral asymmetry on an open space, Phys. Rev. D **30**, 809 (1984).
[60] F. Wilczek and A. Zee, Linking numbers, spin, and statistics of solitons, Phys. Rev. Lett. **51**, 2250 (1983).

[61] J. Goldstone and F. Wilczek, Fractional quantum numbers on solitons, Phys. Rev. Lett. **47**, 986 (1981).
[62] A. Niemi and G. Semenoff, Fermion number fractionization in quantum field theory, Phys. Rep. **135**, 99 (1986).
[63] X.-L. Qi, T. L. Hughes, and S.-C. Zhang, Topological field theory of time-reversal invariant insulators, Phys. Rev. B **78**, 195424 (2008).
[64] M. Stone, C.-K. Chiu, and A. Roy, Symmetries, dimensions and topological insulators: The mechanism behind the face of the bott clock, J. Phys. A: Math. Theor. **44**, 045001 (2011).
[65] A. P. Schnyder, S. Ryu, A. Furusaki, and A. W. W. Ludwig, Classification of topological insulators and superconductors in three spatial dimensions, Phys. Rev. B **78**, 195125 (2008).
[66] A. Karch, D. Tong, and C. Turner, A web of 2d dualities: $\mathbf{Z}_2$ gauge fields and Arf invariants, SciPost Phys. **7**, 007 (2019).
[67] B. A. Bernevig, T. L. Hughes, and S.-C. Zhang, Quantum spin Hall effect and topological phase transition in HgTe quantum wells, Science **314**, 1757 (2006).
[68] We keep results obtained from gapped Q_W so as to ensure ϕ_W well defined.
[69] A. A. Zvyagin, Dynamical quantum phase transitions (Review Article), Low Temp. Phys. **42**, 971 (2016).
[70] M. Heyl, Dynamical quantum phase transitions: A review, Rep. Prog. Phys. **81**, 054001 (2018).
[71] U. Bhattacharya, S. Bandyopadhyay, and A. Dutta, Mixed state dynamical quantum phase transitions, Phys. Rev. B **96**, 180303 (2017).
[72] M. Heyl and J. C. Budich, Dynamical topological quantum phase transitions for mixed states, Phys. Rev. B **96**, 180304 (2017).
[73] J. I. Cirac, D. Pérez-García, N. Schuch, and F. Verstraete, Matrix product states and projected entangled pair states: Concepts, symmetries, theorems, Rev. Mod. Phys. **93**, 045003 (2021).
[74] E. Dennis, A. Kitaev, A. Landahl, and J. Preskill, Topological quantum memory, J. Math. Phys. **43**, 4452 (2002).
[75] M. B. Hastings, Topological order at nonzero temperature, Phys. Rev. Lett. **107**, 210501 (2011).
[76] Y. Bao, R. Fan, A. Vishwanath, and E. Altman, Mixed-state topological order and the errorfield double formulation of decoherence-induced transitions, arXiv:2301.05687.
[77] R. Fan, Y. Bao, E. Altman, and A. Vishwanath, Diagnostics of mixed-state topological order and breakdown of quantum memory, PRX Quantum **5**, 020343 (2024).
[78] J. Y. Lee, Y.-Z. You, and C. Xu, Symmetry protected topological phases under decoherence, Quantum **9**, 1607 (2025).
[79] I. Klich, A note on the full counting statistics of paired fermions, J. Stat. Mech. (2014) P11006.
[80] D. N. Sheng, Z. Y. Weng, L. Sheng, and F. D. M. Haldane, Quantum spin-Hall effect and topologically invariant Chern numbers, Phys. Rev. Lett. **97**, 036808 (2006).
[81] R. Roy, Z_2 classification of quantum spin Hall systems: An approach using time-reversal invariance, Phys. Rev. B **79**, 195321 (2009).
[82] E. Prodan, Robustness of the spin-Chern number, Phys. Rev. B **80**, 125327 (2009).
[83] A. N. Redlich, Gauge noninvariance and parity nonconservation of three-dimensional fermions, Phys. Rev. Lett. **52**, 18 (1984).
[84] S. Ryu, J. E. Moore, and A. W. W. Ludwig, Electromagnetic and gravitational responses and anomalies in topological insulators and superconductors, Phys. Rev. B **85**, 045104 (2012).
[85] X.-L. Qi, Y.-S. Wu, and S.-C. Zhang, Topological quantization of the spin Hall effect in two-dimensional paramagnetic semiconductors, Phys. Rev. B **74**, 085308 (2006).
[86] L. Mao, F. Yang, and H. Zhai, Symmetry-preserving quadratic Lindbladian and dissipation driven topological transitions in Gaussian states, Rep. Prog. Phys. **87**, 070501 (2024).
[87] A. Grabsch, Y. Cheipesh, and C. W. J. Beenakker, Pfaffian formula for fermion parity fluctuations in a superconductor and application to Majorana fusion detection, Ann. Phys. **531**, 1900129 (2019).
[88] A. Y. Kitaev, Unpaired Majorana fermions in quantum wires, Phys. Usp. **44**, 131 (2001).
[89] P. Ghosh, J. D. Sau, S. Tewari, and S. Das Sarma, Non-Abelian topological order in noncentrosymmetric superconductors with broken time-reversal symmetry, Phys. Rev. B **82**, 184525 (2010).